CHEMISTRY
A EUROPEAN JOURNAL

DOI: 10.1002/chem.201001625

FRET Studies on a Series of BODIPY-Dye-Labeled Switchable Resorcin[4]arene Cavitands

Igor Pochorovski, Benjamin Breiten, W. Bernd Schweizer, and François Diederich*[a]

Abstract: A series of borondipyrromethane (BODIPY)-dye-labeled resorcin[4]arene cavitands **1**–**4** with different lengths of oligo(phenylene–ethynylene) spacers between the dyes and the macrocyclic rim has been synthesized. Their switching behavior from the "vase" to "kite" conformations in bulk solution was examined by both variable-temperature (VT) NMR and fluorescence spectroscopy. Both VT-NMR and VT fluorescence resonance energy transfer (FRET) experiments showed that cavitands **1**–**4** undergo vase-to-kite switching at low temperatures. Acid-triggered switching to the kite conformation was observed by fluorescence spectroscopy. Quantitative evaluation of the FRET data led to the determination of the Förster radius $R_0 = 37$ Å for the BODIPY-dye FRET pair and an average cavitand opening angle $\alpha = 16°$ in the vase conformation.

Keywords: cavitands · conformation analysis · FRET · molecular devices · molecular switches

Introduction

Among various classes of receptor molecules, the quinoxaline-bridged resorcin[4]arene cavitands, which were first introduced by Cram and co-workers in 1982, are particularly fascinating because of their ability to undergo a triggered conformational transition from a contracted "vase" state to an expanded "kite" state.[1] To parlay such dynamic behavior into advanced materials that serve as molecular grippers, switches, or receptors, fundamental studies on these cavitand systems are essential.[2] Three types of stimuli have been shown to induce the vase-to-kite transition in the quinoxaline-bridged cavitands: changes in temperature,[1,3,4] pH,[5] and Zn^{II} ion concentration.[6] At ambient temperature, neutral pH, or in the absence of Zn^{II} ions, the closed vase geometry is preferred, whereas lowering the temperature, acidification, or addition of Zn^{II} ions induces the transition to the open kite conformation.

Growing interest in the functionalization of the cavitand system for various applications[2] led to the development of synthetic methods for the preparation of partially and differently bridged resorcin[4]arene cavitands.[7–10] Based on these methods, donor–acceptor borondipyrromethane (BODIPY)-dye[11]-substituted cavitand **1** was prepared, allowing investigations on the mechanism of the vase–kite switching process through fluorescence resonance energy transfer (FRET) studies (Figure 1).[9,12,13] These investigations exploited the fact that the energy-transfer process between the donor and the acceptor dye is strongly dependent on the distance between the two chromophores. Hence, the transition to the kite conformation upon addition of trifluoroacetic acid (TFA) was clearly demonstrated by FRET measurements, as the donor intensity strongly increased and the acceptor intensity almost disappeared, due to the increased distance between the two dyes. However, an unexpectedly low FRET efficiency was observed in the contracted state; because the dyes were assumed to be in close proximity to one another (based on models derived from X-ray structures of quinoxaline-bridged resorcin[4]arene cavitands), a high FRET efficiency was expected. This surprising result was attributed to either the dynamic behavior of the cavitand or an unfavorable orientation of the transition dipole moments of the dyes.[9,13] A separate investigation on dipyrene- and dianthracene-substituted cavitands strengthened the hypothesis that a large conformational flexibility is inherent to these cavitand systems.[14] Both cavitands were shown to form excimers in the vase conformation by means of fluorescence spectroscopy. Opening of these cavitands to the kite state was induced by acidification, presumably imparting a large distance between the fluorophore moieties. Con-

[a] I. Pochorovski, B. Breiten, Dr. W. B. Schweizer, Prof. Dr. F. Diederich
Laboratorium für Organische Chemie
ETH Zürich, Hönggerberg, HCI
8093 Zürich (Switzerland)
Fax: (+41) 44-632-1109
E-mail: diederich@org.chem.ethz.ch

Supporting information for this article is available on the WWW under http://dx.doi.org/10.1002/chem.201001625.

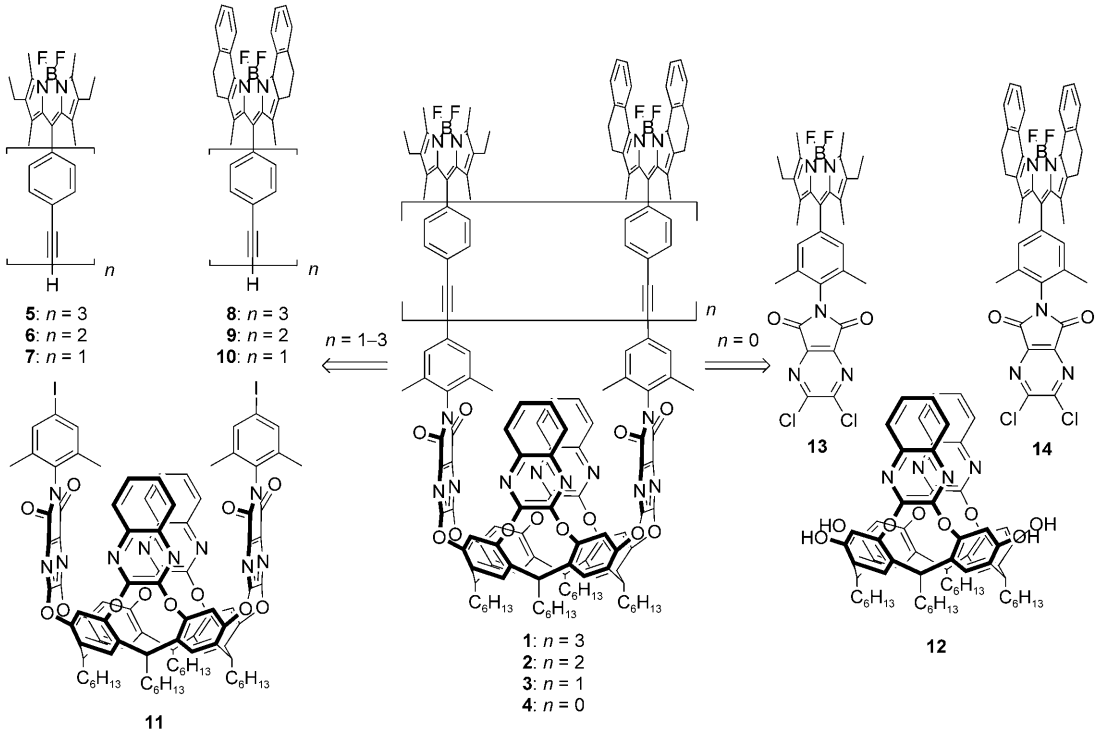

Figure 1. The synthesis of the target cavitands **1**–**4**.

trary to expectations, however, excimer formation did not cease under these conditions. The surprising observations in both studies suggested a high degree of flexibility of the cavitand system.

In light of these results, we decided to investigate the cavitand dynamics in greater detail. Because the Förster radius of the BODIPY-dye pair for a fixed orientation in the cavitand system was unknown, we prepared a series of BODIPY-dye-labeled resorcin[4]arene cavitands **1**–**4**, which incorporate oligo(phenylene–ethynylene) spacers of varying lengths (Figure 1). This series enabled us to correlate the FRET efficiency with the absolute distances between the donor and acceptor dyes and thus to determine the Förster radius and the average solution-state opening angle of the cavitand system.

Results and Discussion

Synthesis of cavitands 1–4: Two different synthetic routes were employed for the preparation of the target cavitands **1**–**4** (Figure 1). Relying on the reported procedure for cavitand **1**, cavitands **1**–**3** were prepared by Sonogashira cross-coupling of the donor dyes **5**–**7** and acceptor dyes **8**–**10** with a common cavitand intermediate, diiodocavitand **11**.[9,14] The smallest cavitand **4** was prepared from bridging tetrol **12**[7,8,10] with flap-attached BODIPY dyes **13** and **14**.

To access diiodocavitand **11**, iodoimide **15**[9] was treated with tetrol **12**[10] in a nucleophilic substitution reaction to afford the desired product, as well as partially bridged cavitand **16** as a side product (Scheme 1). Crystals of both prod-

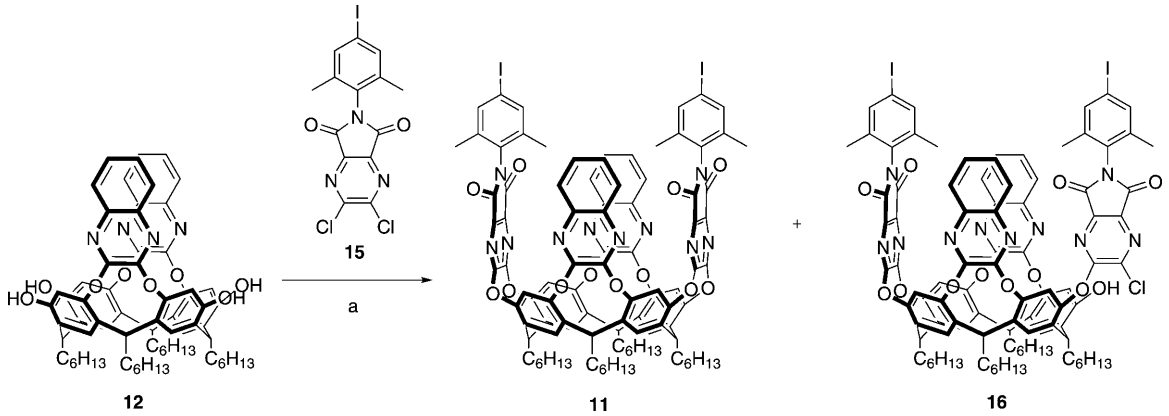

Scheme 1. Synthesis of diiodocavitand **11**. a) K_2CO_3, Me_2SO, 35 °C, 48 h; 38 % (**11**).

ucts were grown from a single acetone/CH_2Cl_2 solution containing a mixture of both compounds (Figure 2).[15]

To prepare the oligo(phenylene–ethynylene)-conjugated BODIPY arms for cavitands **1**–**3**, the short donor-dye arm **7**[9] was treated with phenylacetylenes **17** and **18** (Scheme 2) to give **19**[9] and **20**, respectively.[16] Subsequent alkyne deprotection afforded the two elongated donor-dye arms, **5**[9] and **6**, respectively. In a similar sequence of reactions, elongated acceptor-dye derivatives **8**[9] and **9** were obtained from the short acceptor BODIPY dye **10**[9] after deprotection of **21**[9] and **22**, respectively (Scheme 3).

Following the procedure for the formation of **23**,[9,13] donor arms **6** and **7** were each coupled to diiodocavitand **11** to yield **24** and **25**, respectively (Scheme 4). Compared to the purification of **23** and **24**, purification of **25** was tedious due to its poor solubility in $CHCl_3$; however, recycling gel permeation chromatography (GPC) afforded clean samples of all three monosubstituted cavitands. In the next step, the acceptor arms **8**–**10** were affixed to the monosubstituted cavitands **23**–**25**, affording target cavitands **1**–**3**, which were also purified using recycling GPC.

In the smallest cavitand **4**, the BODIPY dyes are directly affixed to the phenyl linker, thereby necessitating a separate synthesis of quinoxaline-substituted BODIPY arms. Toward this goal, alcohol **26**[17] was oxidized with pyridinium chlorochromate (PCC) and the resulting aldehyde **27** was treated with 3-ethyl-2,4-dimethyl-1*H*-pyrrole in a three-step sequence, yielding BODIPY dye **28** (Scheme 5). Dye **29** was obtained in a similar fashion by reaction of aldehyde **27** with pyrrole **30**.[11b] Crystals of **28** were obtained by evaporation from CH_2Cl_2 (the X-ray structure of **28** is shown in Figure 2SI in the Supporting Information).

To condense the BODIPY-dye moiety with the quinoxaline flap of the cavitand, nitroarenes **28** and **29** were reduced to the corresponding aniline derivatives, **31** and **32**, respectively, using hydrazine and Pd/C[18] (Scheme 5). Aniline-dye derivatives **31** and **32** were then each condensed with anhydride **33**[8,19] to afford dye arms **13** and **14**, respectively (Scheme 6). Crystals of both **13** and **14** were obtained by slow evaporation from CH_2Cl_2. The X-ray structure of **13** is shown in the Supporting Information (Figure 3SI), the one

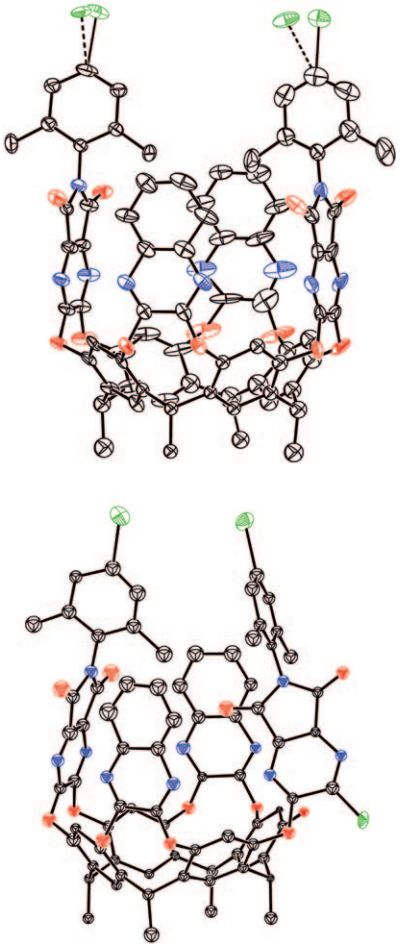

Figure 2. Molecular structures of diiodocavitand **11** (top) and partially bridged cavitand **16** (bottom) in the crystal measured at 123 K. Solvent molecules, *n*-hexyl chains, and hydrogen atoms are omitted for clarity in both cases. Thermal ellipsoids are shown at the 20% probability level for **11** and at the 50% probability level for **16**.

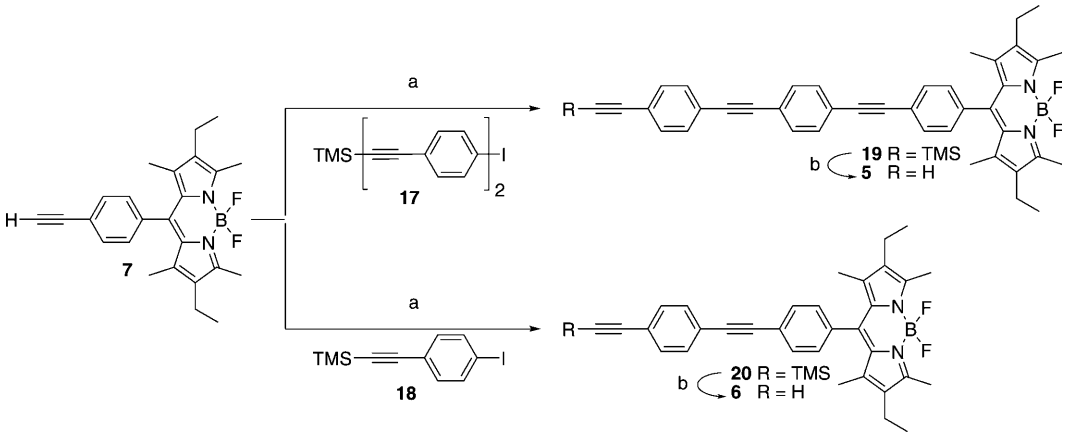

Scheme 2. Synthesis of donor-dye arms **5** and **6**. a) [$Pd(PPh_3)_4$], CuI, *i*Pr_2NEt, THF, 23°C, 2–5 d; 85% (**19**), 77% (**20**). b) *n*Bu_4NF, THF, −78°C, 30 min; 96% (**5**), 77% (**6**). THF = tetrahydrofuran.

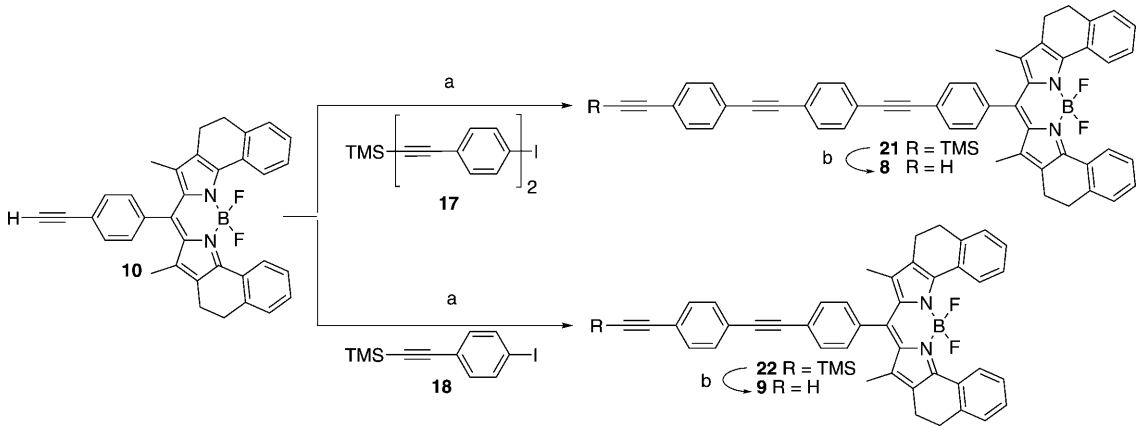

Scheme 3. Synthesis of acceptor-dye arms **8** and **9**. a) $[Pd(PPh_3)_4]$, CuI, iPr$_2$NEt, THF, 23 °C, 2–5 d; 68 % (**21**), 72 % (**22**). b) nBu$_4$NF, THF, −78 °C, 30 min; 79 % (**8**), 86 % (**9**).

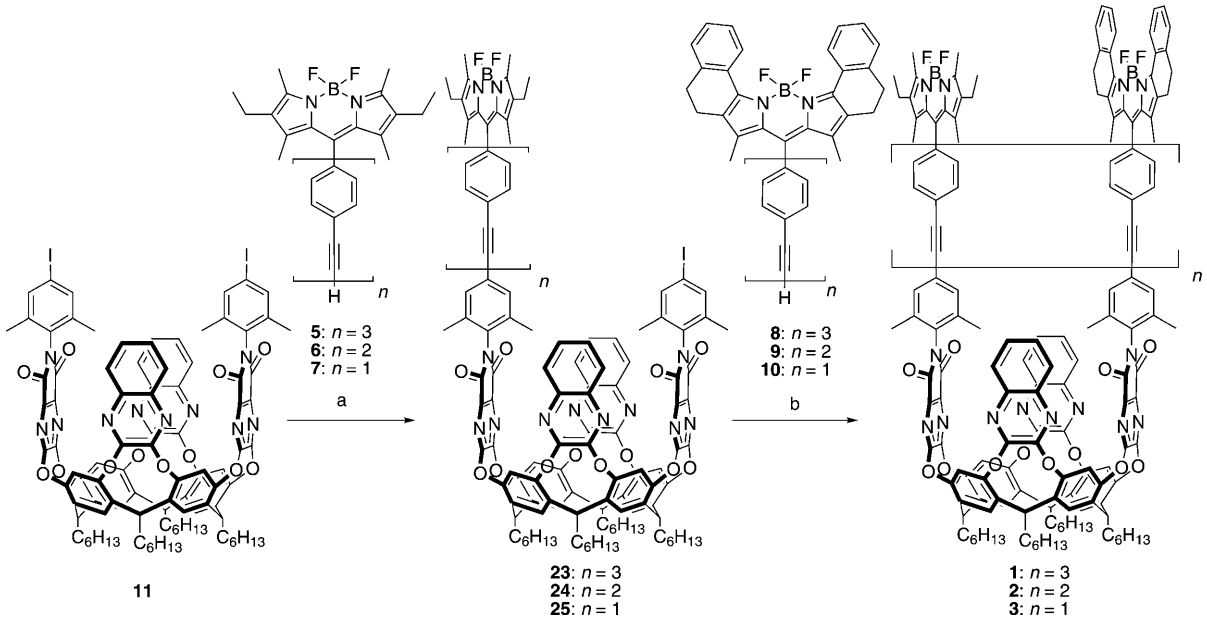

Scheme 4. Synthesis of target cavitands **1**–**3**. a) $[Pd(PPh_3)_4]$, CuI, iPr$_2$NEt, THF, 23 °C, 2–5 d; 26 % (**23**), 24 % (**24**), 22 % (**25**). b) $[Pd(PPh_3)_4]$, CuI, iPr$_2$NEt, THF/CHCl$_3$, 35 °C, 2–5 d; 30 % (**1**), 39 % (**2**), 45 % (**3**).

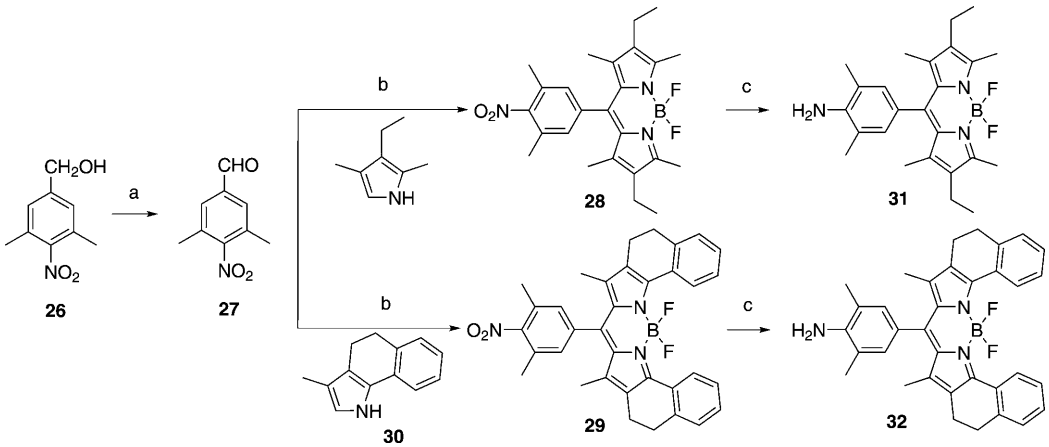

Scheme 5. Synthesis of BODIPY dyes **31** and **32**. a) PCC, CH_2Cl_2, 23 °C, 1 h; 89 % (**27**). b) 1) TFA, CH_2Cl_2, 23 °C, 3 h. 2) DDQ, toluene, 23 °C, 1 h, then NEt_3, $BF_3{\cdot}Et_2O$, 75 °C, 40 min; 70 % (**28**), 69 % (**29**). c) $N_2H_4{\cdot}H_2O$, Pd/C, THF/EtOH, 70 °C, 1–32 h; 92 % (**31**), 51 % (**32**). PCC = pyridinium chlorochromate, TFA = trifluoroacetic acid, DDQ = 2,3-dichloro-5,6-dicyano-*p*-benzoquinone.

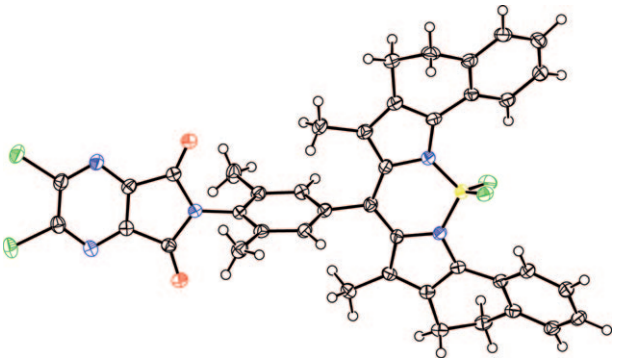

Figure 3. Molecular structure of BODIPY-dye arm **14** in the crystal measured at 123 K. A disordered CH_2Cl_2 molecule is omitted for clarity. Thermal ellipsoids are shown at the 50% probability level.

of **14** is depicted in Figure 3. The dimethylphenyl rings in the two structures are nearly orthogonal to both the BODIPY and pyrazinedione planes. Upon introduction of **13** and **14** into cavitand **4**, such alignment should ensure a parallel arrangement of the two BODIPY dyes, leading to electronic decoupling of the BODIPY moiety from the phenyl linker and an optimum transition dipole orientation for FRET.

In the final assembly of cavitand **4**, BODIPY dyes **13** and **14** were attached to tetrol **12** using standard conditions (K_2CO_3, Me_2SO)[7] (Scheme 7). Donor-dye-substituted cavitand **34** was obtained under these conditions in only 6% yield. MALDI (matrix-assisted laser-desorption-ionization) mass spectra of crude product mixtures from this reaction suggest that the low yield can be attributed to polymerization of the product, in which the free phenolic hydroxy groups of a given molecule of **34** attack the quinoxaline moiety in other molecules **34**. Gratifyingly, the subsequent bridging reaction with dye arm **14** was substantially higher yielding and afforded cavitand **4** in 66% yield.

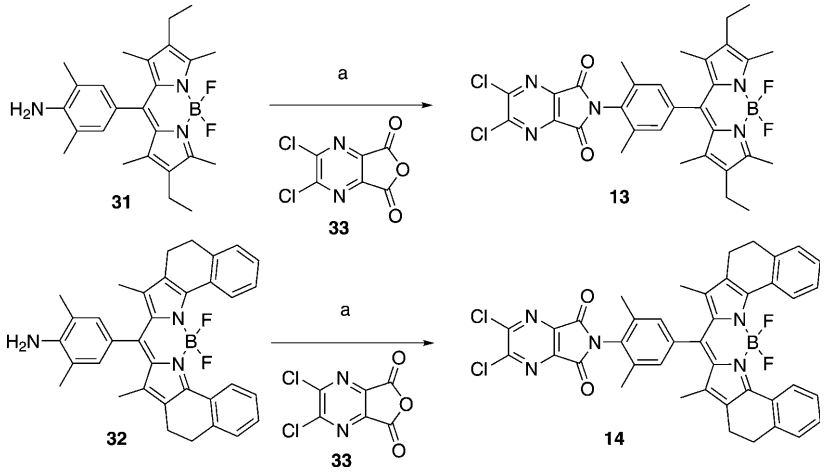

Scheme 6. Synthesis of dye arms **13** and **14**. a) THF, 40°C, 30 min, then $(COCl)_2$, pyridine, 50°C, 16 h; 98% (**13**), 99% (**14**).

Temperature-triggered switching of cavitands 1–4 monitored by ^{1}H and ^{19}F NMR spectroscopy: The vase-to-kite transitions for cavitands **1–4** were conveniently monitored by variable-temperature (VT) ^{1}H NMR spectroscopy (see Figures 5SI–8SI in the Supporting Information).[9] Above 330 K, the methine protons in the octol bowl appear around 5.5 to 5.6 ppm, which is indicative of the vase conformation. Cooling the sample to below 230 K resulted in a diagnostic shift of these

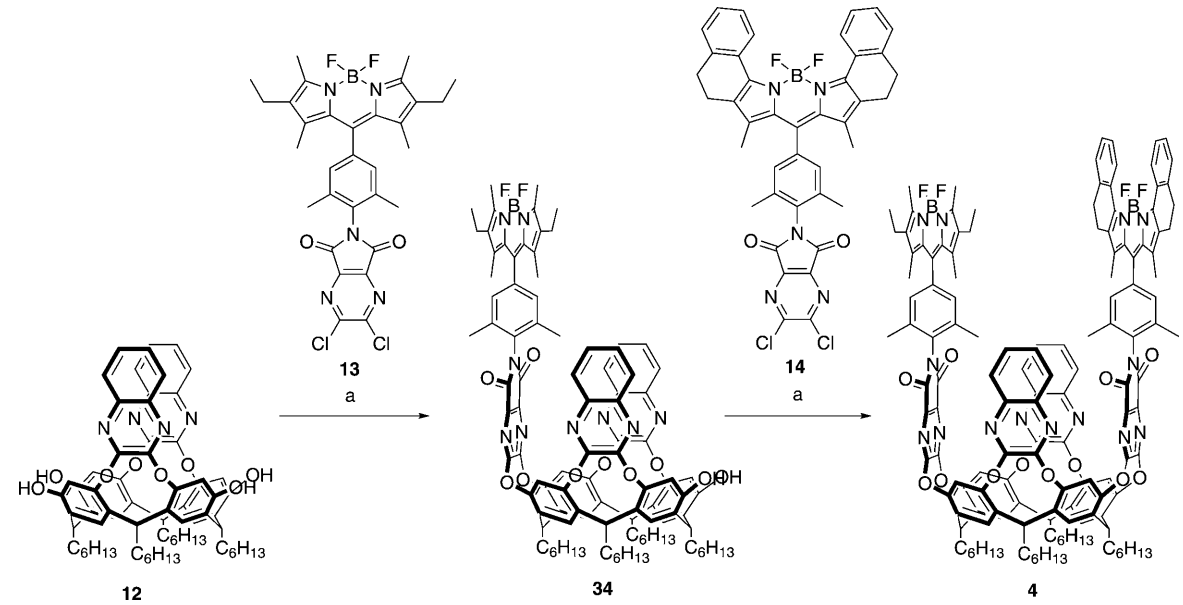

Scheme 7. Synthesis of cavitand **4**. a) K_2CO_3, Me_2SO, 23°C, 4 h; 6% (**34**), 66% (**4**).

methine protons to about 3.7 ppm, consistent with the prevalence of the kite geometry.

We were initially puzzled by a difference observed in the ^{19}F NMR spectra (376 MHz) at 298 K of cavitands **1**–**3** and of cavitand **4** (Figure 4). For cavitands **1**–**3**, a quartet at

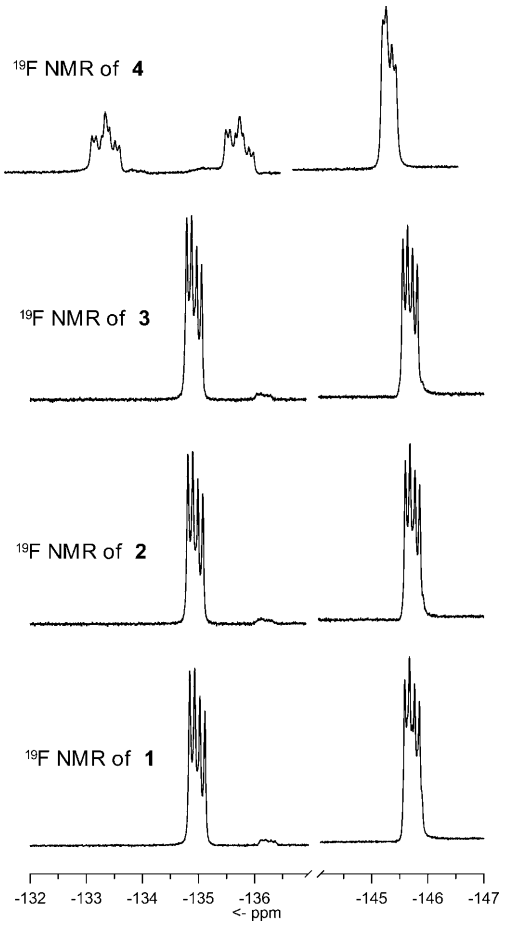

Figure 4. ^{19}F NMR spectra (282 MHz) of cavitands **1**–**4** in $CDCl_3$ at 298 K.

−145 ppm corresponds to the BF_2 unit of the donor dye and another quartet at −135 ppm arises from the BF_2 unit of the acceptor; the quartet splitting pattern of both signals results from $^1J_{BF}$ coupling. The ^{19}F NMR spectrum of cavitand **4** also exhibits a quartet at −145 ppm for the BF_2 unit of the donor dye. For the BF_2 unit of the acceptor dye, however, two sets of overlapping doublets of quartets are observed. The presence of the two signals and their splitting pattern suggest that the two fluorine atoms in the acceptor BODIPY dye are not equivalent; thus, each fluorine atom couples not only to the neighboring boron atom ($^1J_{BF}$), but also to the other fluorine atom ($^2J_{FF}$). To explain the non-equivalence of these fluorine atoms, closer examination of the acceptor BODIPY-dye conformation in cavitand **4** was necessary.

In literature reports on similar BODIPY dyes, the pyrrole wings are canted in the same direction (*syn*) to form an arch-shaped structure, a conformation that renders the two fluorine atoms distinct from one another.[11b,20] The barrier for the interconversion between *syn* and *anti* conformations for the free acceptor dye is relatively low (^{19}F NMR spectra of simple acceptor BODIPY-dye derivatives include only one signal, and the X-ray crystal structure of BODIPY-dye arm **14** shows it in an *anti* conformation, Figure 3). When the acceptor-dye arm is incorporated into cavitand **4**, however, close spatial interactions between the donor and acceptor dyes apparently lock the acceptor dye into a *syn* conformation. Furthermore, unlike in the extended cavitands **1**–**3**, rotation of the BODIPY moieties in cavitand **4** is likely to be more restricted due to methyl groups at both the BODIPY core and the phenyl unit. To test this hypothesis, we performed VT ^{19}F NMR experiments[21] on cavitand **4**, hoping to observe coalescence of the two acceptor dye signals at lower temperatures when the kite geometry puts the donor and acceptor dyes at a greater distance. Indeed, as illustrated in Figure 5, two signals are observed for the BF_2 unit of the acceptor dye in cavitand **4** at 333 K, but only a single broad peak at about −135 ppm is apparent upon cooling the sample to 213 K. In the kite conformation at lower temperatures, the acceptor dye is no longer locked in an arch-shaped conformation and rapid *syn*–*anti* fluctuation in the BODIPY dye renders the two fluorine atoms equivalent on the NMR timescale.

Room-temperature UV/Vis and fluorescence spectroscopy: The UV/Vis spectra of cavitands **1**–**4** exhibit three main ab-

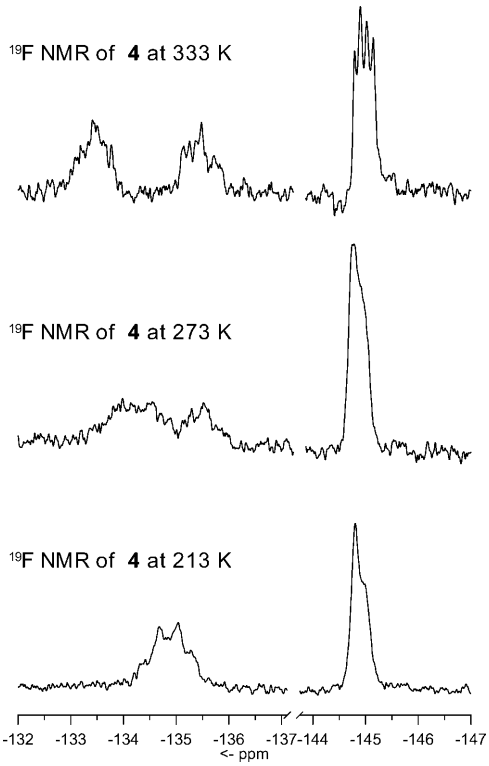

Figure 5. ^{19}F NMR spectra (282 MHz) of cavitand **4** in CD_2Cl_2 at different temperatures (213, 273, 333 K). Exponential apodization of 8.00 Hz along t_1 was used for spectrum processing.

sorption bands corresponding to the oligo(phenylene–ethynylene) spacers ($\lambda = 300$–350 nm), the donor-dye moieties ($\lambda_{max} = 529$ nm), and the acceptor-dye moieties ($\lambda_{max} = 619$ nm) (Figure 6, top). As the number of phenylene–ethynylene moieties in the spacers increases from **4** to **1**, stronger absorption bands in the corresponding part of the UV/Vis spectra are observed.

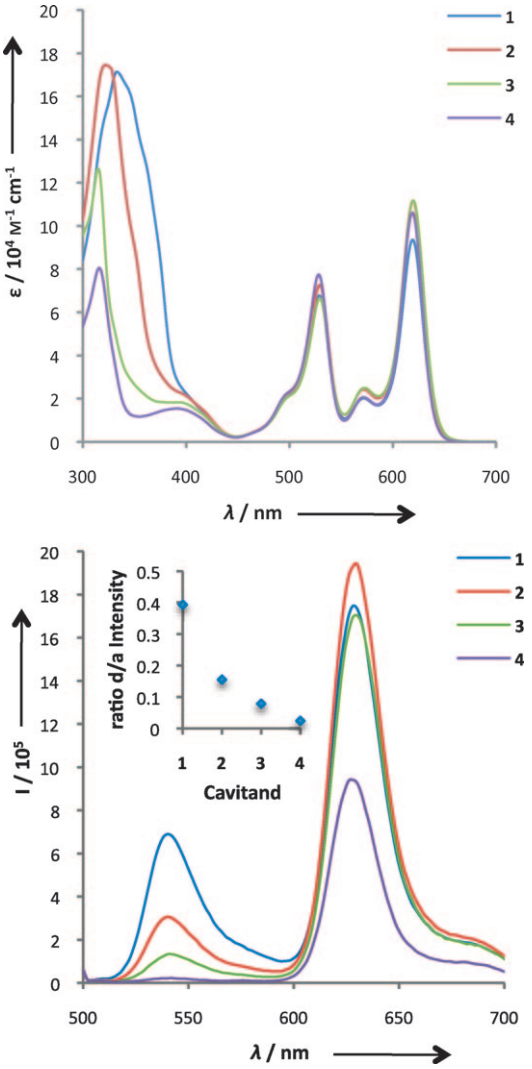

Figure 6. Top: UV/Vis spectra of cavitands **1**–**4** in $CHCl_3$ at 298 K. Bottom: Fluorescence spectra of cavitands **1**–**4** in $CHCl_3$ at 298 K ($c = 0.5 \times 10^{-7}$ M, $\lambda_{exc} = 490$ nm) with graph showing the ratios in the donor/acceptor (d/a) dye emission intensity for cavitands **1**–**4**.

The fluorescence spectra of cavitands **1**–**4** are presented in Figure 6 (bottom); they were recorded in $CHCl_3$ at 298 K with an excitation wavelength of $\lambda_{exc} = 490$ nm, at which only the donor dye is excited. The emission maxima at $\lambda_{em} = 542$ nm correspond to the donor and those at $\lambda_{em} = 630$ nm to the acceptor-dye moieties. A notable conclusion can be drawn from the fluorescence spectra: the ratio of donor/acceptor emission increases with increasing cavitand size. This suggests that the two arms of the cavitands are separated by a certain average opening angle and are not aligned parallel. Greater distances separate the dyes on cavitands with longer arms, correlating to decreased FRET and an increased ratio of donor/acceptor emission intensity.

Acid-triggered switching monitored by fluorescence spectroscopy: Figure 9SI (in the Supporting Information) illustrates the fluorescence titration curves for cavitands **1**–**4**. The opening to the kite form upon protonation is accompanied in each case by an increase in the ratio of donor/acceptor emission intensity. Although these data are internally consistent, and in line with previous results,[9,13] acid-mediated degradation of the BODIPY dyes (see Figures 11SI–13SI in the Supporting Information) precludes a quantitative evaluation of these data.[22] Because changes in temperature can also induce the vase-to-kite transition, we turned to this non-destructive and fully reversible switching method for quantitative fluorescence studies.

Temperature-triggered switching of cavitands 1–4 monitored by fluorescence spectroscopy: The temperature-dependent fluorescence spectra of cavitands **1**–**4** were measured in $CHCl_3$ at temperatures ranging from 218 to 298 K (Figure 10SI in the Supporting Information). The vase-to-kite transitions in all four cavitands are indicated by increases in the ratios between donor and acceptor emission intensities upon lowering the temperature. Figure 7 summarizes these

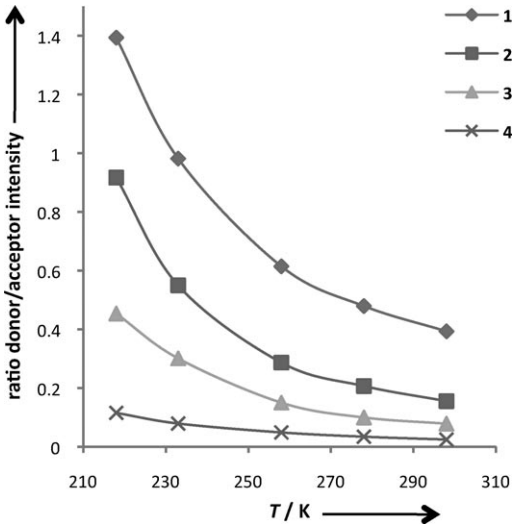

Figure 7. Donor/acceptor dye emission intensities for cavitands **1**–**4** at different temperatures ($c = 0.5 \times 10^{-7}$ M, $\lambda_{exc} = 490$ nm).

results, showing the ratios of donor/acceptor intensities for cavitands **1**–**4**, plotted against temperature. Stronger temperature dependence is correlated to larger phenylene–ethynylene spacer size: the dependence of FRET on temperature is amplified in cavitands with longer arms.

Determination of the average opening angle α and the Förster radius R_0 of cavitands 1–3 in the vase conformation:

The intriguing observation that relative FRET efficiencies of the cavitands in the vase form decrease with increasing phenylene–ethynylene spacer size (Figure 6, bottom) suggests that there is a certain, non-zero average opening angle in the cavitands when they are in the vase conformation. Derivation of this opening angle (α; for definition see Figure 8) and of the Förster radius (R_0)[23] for the donor–acceptor BODIPY-dye pair from fluorescence data will be presented herein. If we assume that the average opening angle α is constant for the four cavitands **1**–**4** at a certain temperature, then the distance between the donor and acceptor BODIPY dyes (R) may be expressed as a function of α and the number of phenylethynyl moieties (n) in the spacer units. The top panel in Figure 8 shows a cavitand that is open with an arbitrary average angle α.

The B–B distance between the boron atoms in the two dyes (R) can be expressed by Equation (1). Using Equations (2) and (3), R can be written as a function of the opening angle α and the number of spacer units n [Equation (4)].

$$R = 2d + a \tag{1}$$

$$d = c\sin(\alpha) \tag{2}$$

$$c = nb + e \tag{3}$$

$$R = 2[(nb + e)\sin(\alpha)] + a = 2e\sin(\alpha) + a + 2b\sin(\alpha)\,n \tag{4}$$

The parameter for the O–O distance, that is $a = 9.6$ Å, was extracted from the X-ray crystal structure of diiodocavitand **11** (Figure 8, bottom). The arm length for $n = 0$, that is, $e = 14.2$ Å, was obtained from the X-ray crystal structures of BODIPY-dye arms **13** and **14**. The length of a single phenylethynyl moiety in the spacers was assumed to be $b = 6.8$ Å, in agreement with X-ray data on 1,4-bis(phenylethynyl)benzene.[24]

Equation (5) enumerates the relationship between the measured FRET efficiency E and the distance R between the BODIPY dyes, with R_0 being the Förster radius. The Förster radius is assumed to be constant for the cavitands **1**–**3** at a given temperature. For cavitand **4**, R_0 is assumed to be distinct from **1**–**3**, owing to the restricted rotation of the dye moieties in **4**, resulting in a different orientation factor. The FRET efficiency E can be calculated from the measured emission intensities of the donor in the presence of the acceptor (I_{DA}, Figure 6, bottom) and in the absence of the acceptor (I_D) [Equation (6)]. For the reference I_D value, the emission intensity of donor-dye arm **20** was used ($c = 0.5 \times 10^{-7}$ M, $\lambda_{exc} = 490$ nm, $I_D = 35 \times 10^5$).

$$E = \frac{1}{1 + \left(\frac{R}{R_0}\right)^6} \tag{5}$$

$$E = 1 - \frac{I_{DA}}{I_D} \tag{6}$$

Equation (5) can be rewritten as Equation (7), which enables the calculation of R/R_0 values from FRET efficiencies. When the expression for R from Equation (4) is substituted into Equation (7), we obtain an expression for R/R_0 that is a linear function of n [Equation (8)].

$$\sqrt[6]{\frac{1}{E} - 1} = \frac{R}{R_0} \tag{7}$$

$$\sqrt[6]{\frac{1}{E} - 1} = \frac{R}{R_0} = \underbrace{\frac{2e\sin(\alpha) + a}{R_0}}_{p} + \underbrace{\frac{2b\sin(\alpha)}{R_0}}_{q} n = p + qn \tag{8}$$

Thus, the plot of R/R_0 versus n can be subjected to a linear fit, from which the slope (q) and a y intercept (p) can be easily obtained. From q and p, the Förster radius R_0 and the opening angle α can be calculated. Figure 9 shows such plot of R/R_0 versus the number of spacer units, n, at 298 K.

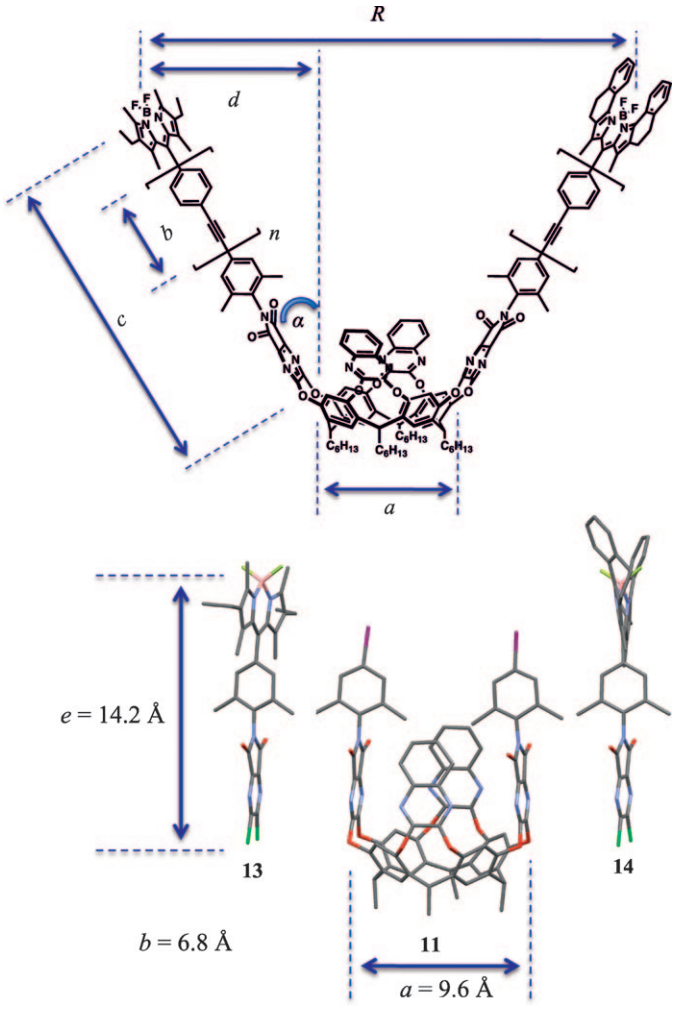

Figure 8. Top: Arbitrary cavitand with oligo(phenylene–ethynylene) spacers at a certain average opening angle α. The B–B distance between the boron atoms in the two BODIPY dyes, R, can be derived from the parameters a, b, and e. Bottom: X-ray crystal structures, from which the parameters e and a were extracted. Parameter b was obtained from X-ray data on 1,4-bis(phenylethynyl)benzene.[24]

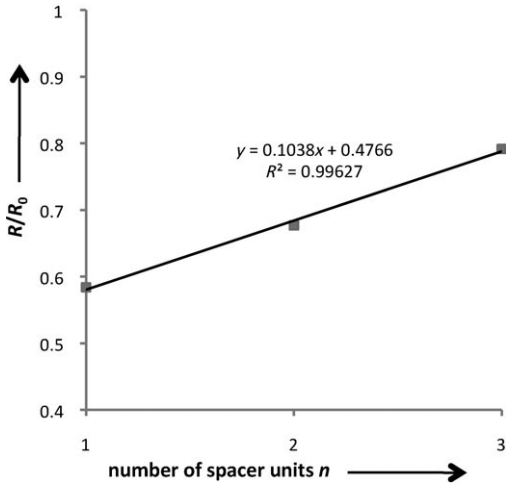

Figure 9. R/R_0 against the number of phenylethynyl units n in the spacer at 298 K.

The linear fit of the plot shows a good correlation ($R^2 = 0.996$), with a slope of $q = 0.104$ and a y intercept of $p = 0.477$. From the slope and y intercept of this line, values for the Förster radius and the average opening angle can be calculated: $R_0 = 37$ Å and $\alpha = 16°$. The value for α is in good agreement with the opening angle range of 0–29° determined by sum-frequency vibrational spectroscopy.[25] Thus, the average distances between the dye moieties in vase-shaped cavitands **1**–**3** at 298 K in $CHCl_3$ range between 21 Å for cavitand **3** and 29 Å for cavitand **1**.

The determined solution-state opening angle is much higher than that in the solid state, observed in the crystal structures of diiodocavitand **5** (Figure 2, top). Indeed, in the solid state, the cavitand walls are directed inwards, resulting in a small, negative opening angle of −2°. Thus, FRET investigations have provided important insights about the vase-type conformation of our cavitands in bulk solution.

Conclusion

A series of BODIPY-dye-labeled resorcin[4]arene cavitands with different lengths of oligo(phenylene–ethynylene) spacers (**1**–**4**) was synthesized. In addition to full characterization of the new cavitands (including UV/Vis and fluorescence spectroscopic characterization), X-ray crystal structures of important synthetic intermediates were obtained. These data provided essential molecular distance parameters that were later used to deduce quantitative information about the vase conformation of the cavitands in bulk solution. Upon obtaining the desired target cavitands, their vase-to-kite switching behavior was observed by both NMR and fluorescence spectroscopy; acid-triggered switching was monitored by fluorescence spectroscopy, and both VT-NMR and VT-FRET experiments confirmed temperature-triggered switching of all four cavitands. Because a series of cavitands could be prepared, a quantitative evaluation of the FRET data was possible and provided new insights into the conformations of these cavitands in solution. Together with the distance parameters obtained from X-ray crystal structures, the quantitative FRET data obtained from the cavitand series enabled determination of the Förster radius for the BODIPY-dye FRET pair ($R_0 = 37$ Å) and the average cavitand opening angle in the vase conformation ($\alpha = 16°$). In contrast to the small opening angle apparent in X-ray crystal structures,[2] such as of vase-cavitand **11**, our studies show that the average opening angle in solution is, in fact, considerably larger. Further time-resolved FRET studies on these cavitand systems are planned to examine their conformational flexibility in solution.

Experimental Section

Materials and general methods: All chemicals were purchased as reagent grade and used without further purification. All solvents for fluorescence spectroscopy were HPLC grade. All reactions were performed in standard glassware under an inert atmosphere of Ar. When stated, solvents were degassed by bubbling Ar through the solution for 30 min. Flash chromatography (FC) was performed using SiO_2-60 (230–400 mesh ASTM, 0.040–0.063 mm; Fluka) or SiO_2-F60 (0.040–0.063 mm, 60 Å, Silicycle). Melting points were measured on a Büchi B-540 melting-point apparatus in open capillaries and are uncorrected. The melting points of the deeply colored BODIPY derivatives could not be accurately determined. Preparative recycling gel permeation chromatography (GPC) was run on a Japan Analytical Industries LC-9101 preparative recycling HPLC apparatus using HPLC-grade $CHCl_3$ as the mobile phase and Jaigel-2H as the stationary phase with a flow of 5 mL min^{-1}. ^{1}H NMR, ^{13}C NMR, and ^{19}F NMR spectra were recorded on a Bruker DRX 400 or Bruker AV 400 spectrometer at 298 K. Residual solvent peak was used as an internal reference. Infrared spectra (IR) were recorded on a Varian 800 FT-IR spectrometer. The spectra were measured neat. Selected absorption bands are reported in wavenumbers (cm^{-1}). Mass spectrometry was performed by the MS-service at ETH Zürich. High-resolution electron impact mass spectra were measured on a Waters Micromass AutoSpec Ultima spectrometer. High-resolution matrix-assisted laser-desorption-ionization mass spectra were measured on a Varion Ionspec Ultima MALDI-FTICR mass spectrometer with 3-hydroxypyridine-2-carboxylic acid (3-HPA) as matrix or on Bruker Daltonics Ultraflex II MALDI-TOF mass spectrometer with (2-[(2*E*)-3-(4-*tert*-butylphenyl)-2-methylprop-2-enyliden]malononitrile) (DCTB) as matrix. High-resolution electro-spray-ionization mass spectra were measured on a Bruker Daltonics maXis spectrometer. Isotope peaks with the highest relative abundance are reported. UV/Vis spectroscopy was carried out with a Varian Cary 500 Scan spectrophotometer. Fluorescence spectroscopy was carried out with an Instruments S. A. Fluorolog-3 spectrofluorimeter. Both UV/Vis and fluorescence experiments were carried out in standard 3.5 mL quartz cells (4 optical windows for UV/Vis, 2 optical windows for fluorescence) with 10 mm path length.

X-ray analysis: All measurements were performed on a Bruker-Nonius Kappa-CCD diffractometer with graphite monochromator and $Mo_{K\alpha}$ radiation, $\lambda = 0.7107$ Å. The structures were solved by direct methods (SIR-97)[26] and refined by full-matrix least-squares analysis (SHELXL-97).[27] All non-hydrogen atoms were refined with anisotropic ADPs. Hydrogen positions were calculated and included in the structure factor calculation.

X-ray crystal structure of ***11***: Crystal data at 123 K for $C_{96}H_{88}I_2N_{10}O_{12}\cdot CH_2Cl_2\cdot 4(C_3H_6O)$, $M_r = 2144.87$, monoclinic, space group $P2_1/c$, $\rho_{calcd} = 1.371$ g cm^{-3}, $Z = 4$, $a = 21.5466(6)$, $b = 25.6543(4)$, $c = 20.0679(5)$ Å, $\alpha = 90.00$, $\beta = 110.4544(10)$, $\gamma = 90.00°$, $V = 10393.4(4)$ Å^3, $\lambda = 0.7107$ Å, $\mu = 0.065$ mm^{-1}. Green-yellow cube (linear dimensions ca. $0.27 \times 0.18 \times 0.135$ mm). Number of measured and unique reflections: 39019 and 12291, respectively ($R_{int} = 0.106$). Disordered structure: I

atoms and some of the *n*-hexyl substituents refined over two positions. Part of an *n*-hexyl substituent could not be localized and was left out; no H atoms were included. Because of poor data, only part of the non-hydrogen atoms refined anisotropically. Geometric restraints were placed on *n*-hexyl fragments. Four acetone and one CH_2Cl_2, as most probable solvent molecules, were included in refinement. Final $R(F)=0.1885$, $wR(F^2)=0.3709$ for 1095 parameters and 8619 reflections with $I>2\sigma(I)$ and $2.425<\theta<21.967°$.

X-ray crystal structure of ***13***: Crystal data at 123 K for $C_{31}H_{30}BCl_2F_2N_5O_2$, $M_r=624.327$, triclinic, space group $P\bar{1}$, $\rho_{calcd}=1.411\ g\,cm^{-3}$, $Z=2$, $a=11.612(4)$, $b=11.745(4)$, $c=12.4611(5)$ Å, $\alpha=86.534(10)$, $\beta=77.219(13)$, $\gamma=62.60(2)°$, $V=1469.7(10)$ Å^3, $\mu=0.273\ mm^{-1}$. Red plate (linear dimensions ca. $0.27\times0.09\times0.015$ mm), bad crystal quality with multiple thin layers giving high mosaic spread. Number of measured and unique reflections: 11725 and 3986, respectively ($R_{int}=0.105$). Final $R(F)=0.1787$, $wR(F^2)=0.3339$ for 396 parameters and 3255 reflections with $I>2\sigma(I)$ and $2.425<\theta<22.986°$.

X-ray crystal structure of ***14***: Crystal data at 123 K for $C_{82}H_{60}BCl_4F_4N_{10}O_4\cdot(CH_2Cl_2)$, $M_r=1573.807$, triclinic, space group $P\bar{1}$, $\rho_{calcd}=1.455\ g\,cm^{-3}$, $Z=1$, $a=7.92060(10)$, $b=12.1909(2)$, $c=20.3353(4)$ Å, $\alpha=102.6460(8)$, $\beta=96.7771(9)$, $\gamma=107.0610(9)°$, $V=1796.32(5)$ Å^3, $\mu=0.312\ mm^{-1}$. Red-brown cube (linear dimensions ca. $0.18\times0.099\times0.069$ mm). Number of measured and unique reflections: 32642 and 8232, respectively ($R_{int}=0.083$). Structure contains one molecule of CH_2Cl_2. Final $R(F)=0.0891$, $wR(F^2)=0.1751$ for 618 parameters and 5924 reflections with $I>2\sigma(I)$ and $2.425<\theta<27.485°$.

X-ray crystal structure of ***16***: Crystal data at 123 K for $C_{96}H_{89}ClI_2N_{10}O_{12}\cdot4(CH_2Cl_2)$, $M_r=2203.79$, monoclinic, space group $P2_1/c$, $\rho_{calcd}=1.483\ g\,cm^{-3}$, $Z=4$, $a=18.2270(3)$, $b=23.1041(5)$, $c=24.2627(5)$ Å, $\alpha=90.00$, $\beta=104.9292(10)$, $\gamma=90.00°$, $V=9872.6(3)$ Å^3, $\mu=0.947\ mm^{-1}$ (numeric absorption correction applied). Green-yellow plate (linear dimensions ca. $0.21\times0.09\times0.03$ mm). Multiple layered, twinned crystal, but no reasonable twin law found. Number of measured and unique reflections: 69005 and 19272, respectively ($R_{int}=0.56$). Only iodine and chlorine atoms refined anisotropically because of limited data quality and overlapping reflexions from the twinning. Structure contains four molecules of CH_2Cl_2. Final $R(F)=0.2788$, $wR(F^2)=0.5603$ for 588 parameters and 10413 reflections with $I>2\sigma(I)$ and $2.425<\theta<26.022°$.

X-ray crystal structure of ***28***: Crystal data at 173 K for $C_{25}H_{30}BF_2N_3O_2$, $M_r=453.341$, monoclinic, space group $P2_1/n$, $\rho_{calcd}=1.258\ g\,cm^{-3}$, $Z=4$, $a=8.5829(3)$, $b=24.5096(7)$, $c=11.5112(3)$ Å, $\alpha=90.00$, $\beta=98.844(2)$, $\gamma=90.00°$, $V=2392.74(12)$ Å^3, $\mu=0.090\ mm^{-1}$. Purple plate (linear dimensions ca. $0.27\times0.225\times0.018$ mm). Number of measured and unique reflections: 17437 and 4340, respectively ($R_{int}=0.109$). Crystal was twinned, refined twinning parameter 0.902:0.098. Final $R(F)=0.1210$, $wR(F^2)=0.2756$ for 299 parameters and 3428 reflections with $I>2\sigma(I)$ and $2.425<\theta<25.350°$.

CCDC-779392 (**11**), -779393 (**13**), -779394 (**14**), -779395 (**16**), and -779396 (**28**) contain the supplementary crystallographic data for this paper. These data can be obtained free of charge from The Cambridge Crystallographic Data Centre via www.ccdc.cam.ac.uk/data_request/cif.

Synthetic procedures: Compounds **1**[9,13], **5**[9], **7**[9], **8**[9], **10**[9], **11**[9], **12**[10], **15**[9], **17**[16], **18**[16], **19**[9], **21**[9], **23**[9], **26**[17], **30**[11b], **33**[8] were prepared according to literature procedures.

Cavitand 2: $[Pd(PPh_3)_4]$ (20 mg, 0.017 mmol) and CuI (3 mg, 0.02 mmol) were added to a degassed solution of **9** (108 mg, 0.172 mmol), **23** (190 mg, 0.0860 mmol), and DIPEA (0.30 mL, 1.7 mmol) in THF (5 mL) and $CHCl_3$ (5 mL). The mixture was stirred for 3 d at 35 °C. The solvent was evaporated. FC (SiO_2; CH_2Cl_2 → CH_2Cl_2/EtOAc 98:2) and recycling GPC (Jaigel-2H; $CHCl_3$) afforded **2** (90 mg, 0.033 mmol, 39%) as a blue solid. $t_R=19.7$ min (Jaigel-2H; $CHCl_3$); ^{1}H NMR (400 MHz, $CDCl_3$): $\delta=$ 0.87–1.02 (m, 18H), 1.28–1.55 (m, 50H), 2.19–2.38 (m, 12H), 2.23 (s, 6H), 2.45–2.56 (m, 10H), 2.85 (t, $J=6.9$ Hz, 4H), 5.62 (t, $J=8.0$ Hz, 2H), 5.70 (t, $J=8.0$ Hz, 2H), 7.27–7.51 (m, 22H), 7.57–7.77 (m, 12H), 7.83–7.94 (m, 4H), 8.25 (s, 4H), 8.80 ppm (d, $J=8.0$ Hz, 2H); ^{13}C NMR (101 MHz, $CDCl_3$): $\delta=12.03$, 12.48, 12.67, 14.22, 14.72, 17.17, 18.19, 18.26, 20.57, 22.81, 28.08, 28.11, 29.50, 29.51, 30.58, 32.01, 32.02, 32.29, 32.81, 34.34, 34.44, 90.43, 90.57, 90.60, 91.02, 118.91, 123.21, 123.25, 123.27, 123.71, 123.91, 123.94, 125.26, 127.48, 128.27, 128.44, 128.51, 128.79, 129.13, 129.25, 129.56, 129.65, 130.63, 131.43, 131.86, 131.87, 131.95, 131.96, 132.32, 132.41, 132.50, 133.18, 133.82, 135.82, 136.26, 136.34, 136.98, 137.56, 138.19, 138.73, 139.14, 139.94, 140.84, 141.61, 151.10, 152.18, 152.37, 153.22, 154.31, 158.98, 161.61 ppm; ^{19}F NMR (376 MHz, $CDCl_3$): $\delta=-145.71$ (q, $J=32.0$ Hz), −134.99 ppm (q, $J=$ 33.0 Hz); IR (ATR): $\tilde{\nu}=2927$, 2857, 2361, 2343, 1740, 1527, 1475, 1444, 1412, 1363, 1326, 1276, 1231, 1191, 1158, 1115, 1082, 1018, 978, 899, 836, 749, 709, 690, 668, 650, 626 cm^{-1}; UV/Vis ($CHCl_3$): λ_{max} (ε) = 323 (175000), 529 (73000), 572 (24000), 620 nm (11200); HR-MALDI-MS (DCTB): *m/z* (%): 2700.1576 (100), $[M]^+$ (calcd for $C_{172}H_{148}B_2F_4N_{14}O_{12}^+$: 2700.1575).

Cavitand 3: $[Pd(PPh_3)_4]$ (24 mg, 0.021 mmol), and CuI (4 mg, 0.02 mmol) were added to a degassed solution of **8** (81 mg, 0.155 mmol), **25** (217 mg, 0.103 mmol), and DIPEA (0.35 mL, 2.1 mmol) in THF (5 mL) and $CHCl_3$ (5 mL). The mixture was stirred for 2 d at 35 °C. The solvent was evaporated. FC (SiO_2; CH_2Cl_2→CH_2Cl_2/EtOAc 98:2) and recycling GPC (Jaigel-2H; $CHCl_3$) afforded **3** (115 mg, 0.046 mmol, 45%) as a blue solid. $t_R=20.4$ min (Jaigel-2H; $CHCl_3$, flow = 4 mL min^{-1}); ^{1}H NMR (400 MHz, $CDCl_3$): $\delta=0.89$–1.01 (m, 18H), 1.31–1.56 (m, 50H), 2.23 (s, 3H), 2.24 (s, 3H), 2.25–2.39 (m, 12H), 2.43–2.55 (m, 10H), 2.84 (t, $J=$ 6.9 Hz, 4H), 5.61 (t, $J=8.0$ Hz, 2H), 5.70 (t, $J=8.1$ Hz, 2H), 7.23–7.55 (m, 22H), 7.72 (d, $J=8.3$ Hz, 2H), 7.77 (d, $J=8.3$ Hz, 2H), 7.87–7.92 (m, 4H), 8.25 (s, 4H), 8.80 ppm (d, $J=8.0$ Hz, 2H); ^{13}C NMR (101 MHz, $CDCl_3$): $\delta=12.03$, 12.48, 12.67, 14.22, 14.72, 17.17, 18.19, 18.26, 20.57, 22.81, 28.08, 28.11, 29.50, 29.51, 30.58, 32.01, 32.02, 32.29, 32.81, 34.34, 34.44, 90.43, 90.57, 90.60, 91.02, 118.91, 123.21, 123.25, 123.27, 123.71, 123.91, 123.94, 125.26, 127.48, 128.27, 128.44, 128.51, 128.79, 129.13, 129.25, 129.56, 129.65, 130.63, 131.43, 131.86, 131.87, 131.95, 131.96, 132.32, 132.41, 132.50, 133.18, 133.82, 135.82, 136.26, 136.34, 136.98, 137.56, 138.19, 138.73, 139.14, 139.94, 140.84, 141.61, 151.10, 152.18, 152.37, 153.22, 154.31, 158.98, 161.61 ppm; ^{19}F NMR (376 MHz, $CDCl_3$): $\delta=-145.66$ (q, $J=31.5$ Hz), −134.97 ppm (q, $J=33.1$ Hz); IR (ATR): $\tilde{\nu}=2927$, 2858, 1740, 1526, 1470, 1411, 1362, 1324, 1276, 1232, 1190, 1157, 1081, 977, 898, 839, 748, 707, 666, 629 cm^{-1}; UV/Vis ($CHCl_3$): λ_{max} (ε) = 315 (126477), 529 (66248), 572 (24984), 620 nm (111728); HR-MALDI-MS (DCTB): *m/z* (%): 2500.0978 (100) $[M]^+$ (calcd for $C_{156}H_{140}B_2F_4N_{14}O_{12}^+$: 2500.0947).

Cavitand 4: K_2CO_3 (10 mg, 0.072 mmol) was added to a degassed solution of **34** (90 mg, 0.055 mmol) and **14** (54 mg, 0.072 mmol) in Me_2SO (6 mL). The mixture was stirred for 4 h at 23 °C, after which it was poured into H_2O (200 mL). The resulting precipitate was collected by filtration, washed with H_2O (3×10 mL), and dried in vacuo. FC (SiO_2; CH_2Cl_2→ CH_2Cl_2/EtOAc 98:2) and recycling GPC (Jaigel-2H; $CHCl_3$) afforded **4** (84 mg, 0.037 mmol, 66%) as a dark blue solid. $t_R=20.7$ min (Jaigel-2H; $CHCl_3$, flow = 4 mL min^{-1}); ^{1}H NMR (400 MHz, $CDCl_3$): $\delta=0.91$–1.01 (m, 18H), 1.31–1.53 (m, 44H), 1.59 (s, 6H), 2.23 (s, 3H), 2.27 (s, 3H), 2.24–2.38 (m, 12H), 2.48 (s, 6H), 2.52–2.66 (m, 4H), 2.89 (t, $J=6.9$ Hz, 4H), 5.61 (t, $J=7.2$ Hz, 2H), 5.69 (t, $J=8.0$ Hz, 2H), 7.14–7.38 (m, 16H), 7.44 (t, $J=7.7$ Hz, 2H), 7.85–7.91 (m, 4H), 8.25 (s, 2H), 8.26 (s, 2H), 8.82 ppm (d, $J=8.0$ Hz, 2H); ^{13}C NMR (101 MHz, $CDCl_3$): $\delta=12.15$, 12.61, 12.70, 14.22, 14.75, 17.24, 18.08, 18.13, 18.38, 18.43, 20.67, 22.81, 28.07, 28.10, 29.50, 29.51, 30.65, 32.01, 32.02, 32.25, 32.86, 34.37, 34.48, 118.90, 123.91, 127.56, 128.22, 128.33, 128.42, 128.68, 128.78, 128.93, 129.13, 129.20, 129.31, 129.52, 129.58, 129.69, 130.50, 132.40, 133.19, 133.69, 135.81, 136.92, 137.05, 137.94, 137.99, 138.07, 138.29, 138.35, 138.40, 138.50, 139.96, 140.82, 141.65, 151.20, 152.19, 152.45, 153.22, 154.52, 158.90, 158.93, 161.31 ppm; ^{19}F NMR (376 MHz, $CDCl_3$): $\delta=$ −146.04, −145.45, −136.63, −135.88, −134.23, −133.51 ppm; IR (ATR): $\tilde{\nu}=2926$, 2857, 2361, 2341, 1741, 1528, 1468, 1444, 1412, 1358, 1325, 1275, 1231, 1189, 1157, 1114, 1101, 1081, 1043, 978, 962, 899, 840, 826, 796, 757, 728, 695, 682, 668; 648 cm^{-1}; UV/Vis ($CHCl_3$): λ_{max} (ε) = 316 (81000), 390 (15000), 528 (77000), 572 (21000), 619 nm (106000); HR-MALDI-MS (DCTB): *m/z* (%): 2300.0361 (100) $[M]^+$ (calcd for $C_{140}H_{132}B_2F_4N_{14}O_{12}^+$: 2300.0319).

{3-Ethyl-5-[(4-ethyl-3,5-dimethyl-2*H*-pyrrol-2-ylidene-κ*N*){4-[(4-ethynylphenyl)-ethynyl]phenyl}methyl]-2,4-dimethyl-1*H*-pyrrolato-κ*N*}(difluoro)boron (6): A solution of **20** (0.65 g, 1.1 mmol) in THF (30 mL) was

cooled to −78 °C. nBu$_4$NF (1 M in THF, 1.4 mL, 1.4 mmol) was added to the solution, and the resulting mixture was stirred for 30 min at −78 °C. Subsequently, AcOH (0.1 mL, 1.7 mmol) was added at −78 °C and the mixture was warmed to 23 °C. The mixture was filtered through a plug of SiO_2, eluted with CH_2Cl_2, and the solvent was removed to afford **6** (0.44 g, 0.87 mmol, 77 %) as a red solid. R_f = 0.30 (SiO_2; CH_2Cl_2/cyclohexane 1:1); m.p.: 235–245 °C (decomp); ^{1}H NMR (400 MHz, $CDCl_3$): δ = 0.99 (t, J = 7.5 Hz, 6H), 1.33 (s, 6H), 2.31 (q, J = 7.5 Hz, 4H), 2.54 (s, 6H), 3.20 (s, 1H), 7.30 (d, J = 8.4 Hz, 2H), 7.46–7.55 (m, 4H), 7.66 ppm (d, J = 8.4 Hz, 2H); ^{13}C NMR (101 MHz, $CDCl_3$): δ = 12.03, 12.68, 14.76, 17.22, 79.29, 83.30, 90.17, 90.83, 122.40, 123.47, 123.67, 128.74, 130.67, 131.66, 132.31, 132.40, 133.11, 136.27, 138.34, 139.29, 154.21 ppm; ^{19}F NMR (376 MHz, $CDCl_3$): δ = −145.78 ppm (q, J = 32.8 Hz); IR (ATR): $\tilde{\nu}$ = 3273, 2963, 2927, 2869, 1537, 1473, 1403, 1388, 1371, 1315, 1263, 1182, 1159, 1115, 1050, 971, 836, 806, 760, 738, 702, 650, 608 cm^{-1}; UV/Vis ($CHCl_3$): λ_{max} (ε) = 302 (39000), 529 nm (74000); HR-MALDI-MS (3-HPA): m/z (%): 504.2549 (100) $[M]^+$ (calcd for $C_{33}H_{31}BF_2N_2^+$: 504.2548), 485.2555 (87) $[M-F]^+$ (calcd for $C_{33}H_{31}BFN_2^+$: 485.2564).

{2-[{4-[(4-Ethynylphenyl)ethynyl]phenyl}(3-methyl-4,5-dihydro-2*H*-benzo[*g*]indol-2-ylidene-κ*N*)methyl]-3-methyl-4,5-dihydro-1*H*-benzo[*g*]indolato-κ*N*}(difluoro)boron (9): A solution of **22** (0.50 g, 0.72 mmol) in THF (60 mL) was cooled to −78 °C. nBu$_4$NF (1 M in THF, 0.9 mL, 0.9 mmol) was added to the solution, and the resulting mixture was stirred for 30 min at −78 °C. Subsequently, AcOH (0.06 mL, 1 mmol) was added at −78 °C and the mixture was warmed to 23 °C. The crude product was washed with $CHCl_3$ (5 mL) and THF (2 mL) to afford **9** (0.39 g, 0.62 mmol, 86 %) as a dark brown-green solid. R_f = 0.44 (SiO_2; CH_2Cl_2/cyclohexane 1:1); m.p.: 330–340 °C (decomp); ^{1}H NMR (400 MHz, $CDCl_3$): δ = 1.41 (s, 3H), 2.54 (t, J = 7.0 Hz, 2H), 2.88 (t, J = 7.0 Hz, 2H), 3.20 (s, 1H), 7.22–7.34 (m, 4H), 7.37–7.47 (m, 4H), 7.48–7.56 (m, 4H), 7.71 (d, J = 8.3 Hz, 2H), 8.81 ppm (d, J = 7.9 Hz, 2H); ^{13}C NMR not available due to low solubility of the solid; ^{19}F NMR (376 MHz, $CDCl_3$): δ = −135.00 ppm (d, J = 33.6 Hz); IR (ATR): δ = 3290, 2939, 2899, 2838, 1604, 1560, 1519, 1466, 1429, 1390, 1368, 1340, 1322, 1308, 1273, 1229, 1190, 1169, 1152, 1109, 1082, 1059, 1042, 1013, 966, 945, 849, 834, 820, 769, 747, 726, 713, 705, 671, 651, 634 cm^{-1}; UV/Vis ($CHCl_3$): λ_{max} (ε) = 320 (95000), 571 (27000), 618 nm (119000); HR-MALDI-MS (3-HPA): m/z (%): 624.2553 (82) $[M]^+$ (calcd for $C_{43}H_{31}BF_2N_2^+$: 624.2548), 605.2560 (100) $[M-F]^+$ (calcd for $C_{43}H_{31}BFN_2^+$: 605.2564).

[2,3-Dichloro-6-{4-[(4-ethyl-3,5-dimethyl-1*H*-pyrrol-2-yl-κ*N*)(4-ethyl-3,5-dimethyl-2*H*-pyrrol-2-ylidene-κ*N*)methyl]-2,6-dimethylphenyl}-5*H*-pyrrolo[3,4-*b*]pyrazine-5,7(6*H*)-dionato](difluoro)boron (13): A solution of **33** (0.90 g, 4.11 mmol) and **31** (1.66 g, 3.91 mmol) in THF (60 mL) was heated to 40 °C for 30 min. After cooling to 23 °C, $(COCl)_2$ (0.40 mL, 4.7 mmol) and pyridine (0.95 mL, 12 mmol) were added and the resulting mixture was stirred for 16 h at 50 °C. The solvent was evaporated, and the crude product was filtered through a plug of SiO_2 and eluted with CH_2Cl_2 to afford **13** (2.39 g, 3.83 mmol, 98 %) as a red solid. R_f = 0.20 (SiO_2; CH_2Cl_2/cyclohexane 3:1); m.p.: 330–340 °C (decomp); ^{1}H NMR (400 MHz, $CDCl_3$): δ = 1.01 (t, J = 7.6 Hz, 6H), 1.43 (s, 6H), 2.20 (s, 6H), 2.33 (q, J = 7.5 Hz, 4H), 2.54 (s, 6H), 7.18 ppm (s, 2H); ^{13}C NMR (101 MHz, $CDCl_3$): δ = 12.18, 12.69, 14.74, 17.26, 18.31, 128.83, 129.10, 130.62, 133.20, 137.87, 138.01, 138.48, 138.69, 143.50, 154.29, 154.49, 160.89 ppm; ^{19}F NMR (376 MHz, $CDCl_3$): δ = −145.81 ppm (q, J = 32.9 Hz); IR (ATR): $\tilde{\nu}$ = 2962, 2929, 2869, 1795, 1733, 1537, 1474, 1404, 1383, 1369, 1316, 1265, 1232, 1186, 1114, 1061, 1043, 974, 869, 830, 812, 758, 744, 712, 630, 611 cm^{-1}; UV/Vis ($CHCl_3$): λ_{max} (ε) = 378 (7000), 529 nm (71000); HR-MALDI-MS (3-HPA): m/z (%): 623.1838 (100) $[M]^+$ (calcd for $C_{31}H_{30}BCl_2F_2N_5O_2^+$: 623.1838), 604.1848 (63) $[M-F]^+$ (calcd for $C_{31}H_{30}BCl_2FN_5O_2^+$: 604.1854).

[2,3-Dichloro-6-{2,6-dimethyl-4-[(3-methyl-4,5-dihydro-1*H*-benzo[*g*]indol-2-yl-κ*N*)(3-methyl-4,5-dihydro-2*H*-benzo[*g*]indol-2-ylidene-κ*N*)methyl]phenyl}-5*H*-pyrrolo[3,4-*b*]pyrazine-5,7(6*H*)-dionato](difluoro)boron (14): A solution of **33** (0.110 g, 0.50 mmol) and **32** (0.213 g, 0.391 mmol) in THF (10 mL) was heated to 40 °C for 30 min. After cooling to 23 °C, $(COCl)_2$ (0.04 mL, 5 mmol) and pyridine (0.01 mL, 1 mmol) were added and the resulting mixture was stirred for 16 h at 50 °C. The solvent was evaporated, and the crude product was filtered through a plug of SiO_2 and eluted with CH_2Cl_2 to afford **14** (0.29 g, 0.39 mmol, 99 %) as a black solid. R_f = 0.25 (SiO_2; CH_2Cl_2/cyclohexane 3:1); m.p.: 310–320 °C (decomp); ^{1}H NMR (400 MHz, $CDCl_3$): δ = 1.50 (s, 6H), 2.24 (s, 6H), 2.57 (t, J = 7.0 Hz, 4H), 2.89 (t, J = 7.0 Hz, 4H), 7.24–7.34 (m, 6H), 7.43 (t, J = 7.0 Hz, 2H), 8.81 ppm (d, J = 8.0 Hz, 2H); ^{13}C NMR (101 MHz, $CDCl_3$): δ = 12.60, 18.34, 20.65, 30.69, 127.50, 128.23, 128.54, 128.87 (t, J = 12.1 Hz), 129.31, 129.33, 129.62, 132.38, 133.81, 136.13, 138.01, 138.28, 138.36, 140.87, 143.52, 151.15, 154.53, 160.90 ppm; ^{19}F NMR (376 MHz, $CDCl_3$): δ = −135.03 ppm (q, J = 34.0 Hz); IR (ATR): $\tilde{\nu}$ = 2926, 1738, 1605, 1549, 1522, 1467, 1434, 1385, 1367, 1339, 1320, 1273, 1231, 1196, 1157, 1080, 1061, 1031, 1013, 961, 908, 874, 829, 812, 767, 742, 728, 714, 705, 650, 627, 610 cm^{-1}; UV/Vis ($CHCl_3$): λ_{max} (ε) = 316 (58000), 395 (9000), 571 (23000), 618 nm (111000); HR-MALDI-MS (3-HPA): m/z (%): 743.1843 (100) $[M]^+$ (calcd for $C_{41}H_{30}BCl_2F_2N_5O_2^+$: 743.1838), 724.1864 (61) $[M-F]^+$ (calcd for $C_{41}H_{30}BCl_2FN_5O_2^+$: 724.1854).

(3-Ethyl-5-{(4-ethyl-3,5-dimethyl-2*H*-pyrrol-2-ylidene-κ*N*)[4-({4-[(trimethylsilyl)ethynyl]phenyl}ethynyl)phenyl]methyl}-2,4-dimethyl-1*H*-pyrrolato-κ*N*)(difluoro)boron (20): $[Pd(PPh_3)_4]$ (0.10 g, 0.087 mmol), and CuI (0.016 g, 0.087 mmol) were added to a degassed solution of **7** (0.70 g, 1.7 mmol), **18** (0.55 g, 1.8 mmol), and DIPEA (1.8 mL, 10 mmol) in THF (50 mL). The mixture was stirred for 3 d at 23 °C, then filtered through Celite and purified by FC (SiO_2; CH_2Cl_2/cyclohexane 1:1) to afford **20** (0.77 g, 1.3 mmol, 77 %) as a red solid. R_f = 0.30 (SiO_2; CH_2Cl_2/cyclohexane 1:1); m.p.: 155–160 °C (decomp); ^{1}H NMR (400 MHz, $CDCl_3$): δ = 0.26 (s, 9H), 0.99 (t, J = 7.5 Hz, 7H), 1.33 (s, 6H), 2.31 (q, J = 7.5 Hz, 4H), 2.54 (s, 6H), 7.29 (d, J = 8.4 Hz, 2H), 7.45–7.51 (m, 4H), 7.65 ppm (d, J = 8.4 Hz, 2H); ^{13}C NMR (101 MHz, $CDCl_3$): δ = 0.06, 12.03, 12.68, 14.74, 17.23, 90.42, 90.78, 96.75, 104.67, 123.05, 123.48, 123.79, 128.76, 130.71, 131.59, 132.14, 132.38, 133.12, 136.24, 138.36, 139.35, 154.22 ppm; ^{19}F NMR (376 MHz, $CDCl_3$): δ = −145.81 (q, J = 33.0 Hz) ppm; IR (ATR): $\tilde{\nu}$ = 2960, 1538, 1474, 1404, 1315, 1249, 1182, 1115, 1072, 975, 835, 759, 705 cm^{-1}; UV/Vis ($CHCl_3$): λ_{max} (ε) = 308 (38000), 529 nm (67000); HR-MALDI-MS (3-HPA): m/z (%): 576.2940 (83) $[M]^+$ (calcd for $C_{36}H_{39}BF_2N_2Si^+$: 576.2944), 557.2956 (100) $[M-F]^+$ (calcd for $C_{36}H_{39}BFN_2Si^+$: 557.2960).

Difluoro(3-methyl-2-{(3-methyl-4,5-dihydro-2*H*-benzo[*g*]indol-2-ylidene-κ*N*)[4-({4-[(trimethylsilyl)ethynyl]phenyl}ethynyl)phenyl]methyl}-4,5-dihydro-1*H*-benzo[*g*]-indolato-κ*N*)boron (22): $[Pd(PPh_3)_4]$ (0.066 g, 0.057 mmol), and CuI (0.011 g, 0.057 mmol) were added to a degassed solution of **10** (0.60 g, 1.14 mmol), **18** (0.36 g, 1.2 mmol), and DIPEA (1.2 mL, 6.9 mmol) in THF (50 mL). The mixture was stirred for 3 d at 23 °C, then filtered through Celite and purified by FC (SiO_2; CH_2Cl_2/cyclohexane 2:3) to afford **22** (0.57 g, 0.82 mmol, 72 %) as a black solid. R_f = 0.55 (SiO_2; CH_2Cl_2/cyclohexane 1:1); m.p.: 265–275 °C (decomp); ^{1}H NMR (400 MHz, $CDCl_3$): δ = 0.27 (s, 9H), 1.40 (s, 6H), 2.54 (t, J = 7.0 Hz, 4H), 2.88 (t, J = 7.0 Hz, 4H), 7.21–7.27 (m, 2H), 7.28–7.35 (m, 2H), 7.37–7.54 (m, 8H), 7.70 (d, J = 8.2 Hz, 2H), 8.81 ppm (d, J = 8.0 Hz, 2H); ^{13}C NMR (101 MHz, $CDCl_3$): δ = 0.06, 12.48, 20.61, 30.66, 90.60, 90.75, 96.79, 104.65, 123.00, 123.50, 124.01, 127.49, 128.22, 128.51, 128.80 (t, J = 11.6 Hz), 129.20, 129.60, 131.61, 132.16, 132.30, 132.47, 133.88, 136.03, 136.55, 138.93, 140.83, 151.06 ppm; ^{19}F NMR (376 MHz, $CDCl_3$): δ = −134.97 ppm (q, J = 32.9 Hz); IR (ATR): $\tilde{\nu}$ = 2933, 2163, 1604, 1556, 1525, 1464, 1435, 1400, 1367, 1326, 1307, 1275, 1231, 1195, 1156, 1118, 1083, 1014, 965, 945, 863, 827, 768, 706, 657, 631 cm^{-1}; UV/Vis ($CHCl_3$): λ_{max} (ε) = 318 (93000), 571 (26000), 618 nm (120000); HR-MALDI-MS (3-HPA): m/z (%): 696.2936 (100) $[M]^+$ (calcd for $C_{46}H_{39}BF_2N_2Si^+$: 696.2944), 677.2969 (68) $[M-F]^+$ (calcd for $C_{46}H_{39}BFN_2Si^+$: 677.2960).

Compound 24: $[Pd(PPh_3)_4]$ (47 mg, 0.041 mmol), and CuI (8 mg, 0.04 mmol) were added to a degassed solution of **6** (155 mg, 0.308 mmol), **11** (0.75 g, 0.41 mmol), and DIPEA (1.4 mL, 8.2 mmol) in THF (30 mL). The mixture was stirred for 2 d at 23 °C, after which the solvent was evaporated. FC (SiO_2; CH_2Cl_2→CH_2Cl_2/EtOAc 98:2) and recycling GPC (Jaigel-2H; $CHCl_3$) afforded **24** (216 mg, 0.098 mmol, 24 %) as a red solid. t_R = 20.6 min (Jaigel-2H; $CHCl_3$, flow = 4 mL min^{-1}); m.p.: 260–270 °C (decomp); ^{1}H NMR (400 MHz, $CDCl_3$): δ = 0.94 (q, J = 6.7 Hz, 12H), 1.00 (t, J = 7.6 Hz, 6H), 1.35 (s, 6H), 1.29–1.56 (m, 38H), 2.17 (s, 3H), 2.23 (s, 3H), 2.20–2.39 (m, 12H), 2.55 (s, 6H), 5.62 (t, J = 7.0 Hz, 2H), 5.70 (t, J = 8.1 Hz, 2H), 7.27–7.35 (m, 10H), 7.46–7.72 (m, 10H),

7.83–7.90 (m, 4H), 8.24 (s, 2H), 8.25 ppm (s, 2H); ^{13}C NMR (101 MHz, $CDCl_3$): δ = 12.06, 12.70, 14.23, 14.79, 17.22, 17.79, 17.95, 18.15, 18.26, 22.81, 28.07, 28.10, 29.51, 29.52, 29.85, 32.00, 32.01, 32.24, 32.79, 34.30, 34.39, 90.40, 90.42, 90.68, 90.92, 91.25, 96.72, 118.88, 123.04, 123.07, 123.28, 123.36, 123.69, 123.87, 125.28, 128.43, 128.50, 128.72, 128.83, 128.98, 129.55, 130.65, 131.79, 131.83, 131.90, 132.41, 133.10, 135.79, 135.81, 136.09, 136.23, 136.94, 136.97, 137.51, 137.54, 137.91, 138.35, 139.26, 139.29, 139.89, 139.90, 141.51, 141.57, 152.12, 152.14, 152.34, 153.18, 154.19, 158.98, 161.46, 161.59 ppm; ^{19}F NMR (376 MHz, $CDCl_3$): δ = −145.77 ppm (d, J = 32.8 Hz); IR (ATR): $\tilde{\nu}$ = 2926, 2857, 2360, 1740, 1539, 1479, 1446, 1412, 1359, 1323, 1258, 1235, 1190, 1157, 1115, 1101, 1064, 979, 898, 837, 760, 709, 689, 668, 618 cm^{-1}; UV/Vis ($CHCl_3$): λ_{max} (ε) = 328 (82000), 529 (69000); HR-MALDI-MS (3-HPA): m/z (%): 2203.8151 (34) $[M]^+$ (calcd for $C_{129}H_{118}BF_2IN_{12}O_{12}^+$: 2203.8132), 2184.8202 (100) $[M-F]^+$ (calcd for $C_{129}H_{118}BFIN_{12}O_{12}^+$: 2184.8151).

Compound 25: $[Pd(PPh_3)_4]$ (47 mg, 0.041 mmol), and CuI (8 mg, 0.04 mmol) were added to a degassed solution of **7** (124 mg, 0.308 mmol), **11** (0.75 g, 0.41 mmol), and DIPEA (1.4 mL, 8.2 mmol) in THF (30 mL). The mixture was stirred for 16 h at 23 °C, after which the solvent was evaporated. FC (SiO_2; CH_2Cl_2→CH_2Cl_2/EtOAc 98:2) and recycling GPC (Jaigel-2H; $CHCl_3$) afforded **25** (192 mg, 0.091 mmol, 22%) as a red solid. t_R = 20.7 min (Jaigel-2H; $CHCl_3$, flow = 4 mL min^{-1}); m.p.: 280–290 °C (decomp); ^{1}H NMR (400 MHz, $CDCl_3$): δ = 0.94 (q, J = 6.7 Hz, 12H), 1.01 (t, J = 7.5 Hz, 6H), 1.38 (s, 6H), 1.29–1.55 (m, 38H), 2.16 (s, 3H), 2.24 (s, 3H), 2.21–2.41 (m, 12H), 2.56 (s, 6H), 5.62 (t, J = 7.1 Hz, 2H), 5.70 (t, J = 8.1 Hz, 2H), 7.27–7.38 (m, 10H), 7.49 (s, 1H), 7.50 (s, 1H), 7.67 (s, 2H), 7.74 (d, J = 8.3 Hz, 2H), 7.83–7.92 (m, 4H), 8.24 (s, 2H), 8.25 ppm (s, 2H); ^{13}C NMR (101 MHz, $CDCl_3$): δ = 12.12, 12.71, 14.22, 14.79, 17.26, 17.83, 17.94, 18.19, 18.27, 22.81, 28.08, 28.11, 29.50, 29.51, 29.85, 32.01, 32.02, 32.29, 32.81, 34.32, 34.42, 89.62, 90.42, 96.67, 118.91, 123.59, 123.90, 125.19, 128.47, 128.53, 128.85, 128.90, 129.14, 129.52, 130.70, 131.60, 132.37, 132.53, 133.16, 135.83, 135.84, 136.17, 136.47, 136.99, 137.01, 137.48, 137.64, 137.94, 138.37, 139.26, 139.31, 139.94, 141.54, 141.61, 152.16, 152.17, 152.38, 153.21, 154.27, 159.01, 161.45, 161.60 ppm; ^{19}F NMR (376 MHz, $CDCl_3$): δ = −145.76 ppm (q, J = 32.4 Hz); IR (ATR): $\tilde{\nu}$ = 2925, 2856, 2361, 2341, 1740, 1712, 1530, 1477, 1444, 1412, 1361, 1327, 1264, 1231, 1191, 1158, 1115, 1101, 1083, 1019, 978, 899, 838, 761, 709, 689, 668, 652, 604 cm^{-1}; UV/Vis ($CHCl_3$): λ_{max} (ε) = 529 (68000); HR-MALDI-MS (3-HPA): m/z (%): 2103.7745 (86) $[M]^+$ (calcd for $C_{121}H_{114}BF_2IN_{12}O_{12}^+$: 2103.7821), 2084.7743 (100) $[M-F]^+$ (calcd for $C_{121}H_{114}BFIN_{12}O_{12}^+$: 2084.7834).

3,5-Dimethyl-4-nitrobenzaldehyde (27): Alcohol **26** (4.47 g, 24.7 mmol) in CH_2Cl_2 (3 mL) was added to a suspension of PCC (9.6 g, 44 mmol) in CH_2Cl_2 (100 mL). The resulting dark suspension was stirred for 1 h at 23 °C after which Et_2O (120 mL) and Celite were added to the reaction mixture to form a black slurry, which was filtered through a plug of SiO_2 and eluted with CH_2Cl_2. Upon removal of solvent, **27** (3.94 g, 22.0 mmol, 89%) was obtained as a tan solid. R_f = 0.41 (SiO_2; CH_2Cl_2/cyclohexane 2:1); m.p.: 50–51 °C (Lit:[28] 52–54 °C); ^{1}H NMR (400 MHz, $CDCl_3$): δ = 2.38 (s, 6H), 7.65 (s, 2H), 9.99 ppm (s, 1H); ^{13}C NMR (101 MHz, $CDCl_3$): δ = 17.38, 130.23, 130.77, 136.81, 155.23, 190.81 ppm; HR-EI-MS (70 eV): m/z: 179.0577 $[M]^+$ (calcd for $C_9H_9NO_3^+$: 179.0582).

{2-[(3,5-Dimethyl-4-nitrophenyl)(4-ethyl-3,5-dimethyl-2*H*-pyrrol-2-ylidene-κ*N*)-methyl]-4-ethyl-3,5-dimethyl-1*H*-pyrrolato-κ*N*}(difluoro)boron (28): A catalytic amount of TFA (0.1 mL, 1 mmol) was added to a solution of **27** (2.0 g, 11 mmol) and 3-ethyl-2,4-dimethyl-1*H*-pyrrole (3.0 g, 23 mmol) in CH_2Cl_2 (700 mL) at 23 °C, and the resulting solution was stirred for 3 h at 23 °C. The solution was washed with a saturated aqueous $NaHCO_3$ solution, brine, dried over $MgSO_4$, and filtered. The solvent was evaporated, and the resulting solid was dissolved in toluene (400 mL). A suspension of DDQ (2.68 g, 11.7 mmol) in toluene (200 mL) was added, and the mixture was stirred for 1 h at 23 °C. Then, TEA (6.3 mL, 45 mmol) and BF_3·Et_2O (8.0 mL, 65 mmol) were added, and the mixture was heated to 75 °C for 40 min. After cooling to 23 °C, the mixture was filtered through a plug of SiO_2, eluted with CH_2Cl_2 and the solvent was evaporated. The crude product was purified by FC (SiO_2; CH_2Cl_2/cyclohexane 2:1) to afford **28** (3.53 g, 7.79 mmol, 70%) as a metallic green solid. R_f = 0.48 (SiO_2; CH_2Cl_2/cyclohexane 1:1); m.p.: 237–250 °C; ^{1}H NMR (400 MHz, $CDCl_3$): δ = 0.99 (t, J = 7.6 Hz, 6H), 1.34 (s, 6H), 2.31 (q, J = 7.6 Hz, 4H), 2.38 (s, 6H), 2.53 (s, 6H), 7.11 ppm (s, 2H); ^{13}C NMR (101 MHz, $CDCl_3$): δ = 12.30, 12.70, 14.71, 17.22, 17.65, 129.10, 130.43, 130.95, 133.36, 137.70, 138.02, 138.09, 152.21, 154.66 ppm; ^{19}F NMR (376 MHz, $CDCl_3$): δ = −145.84 ppm (q, J = 32.9 Hz); IR (ATR): $\tilde{\nu}$ = 2965, 2927, 2869, 1746, 1602, 1526, 1474, 1406, 1368, 1311, 1263, 1222, 1180, 1159, 1117, 1038, 974, 929, 867, 827, 758, 607 cm^{-1}; UV/Vis ($CHCl_3$): λ_{max} (ε) = 379 (8000), 531 nm (73000); HR-MALDI-MS (3-HPA): m/z (%): 453.2397 (100) $[M]^+$ (calcd for $C_{25}H_{30}BF_2N_3O_2^+$: 453.2399), 434.2410 (86) $[M-F]^+$ (calcd for $C_{25}H_{30}BFN_3O_2^+$: 434.2415).

{2-[(3,5-Dimethyl-4-nitrophenyl)(3-methyl-4,5-dihydro-2*H*-benzo[*g*]indol-2-ylidene-κ*N*)methyl]-3-methyl-4,5-dihydro-1*H*-benzo[*g*]indolato-κ*N*}(difluoro)boron (29): A catalytic amount of TFA (0.02 mL, 0.3 mmol) was added and the solution stirred for 3 h at 23 °C, to a solution of **27** (0.50 g, 2.8 mmol) and **30** (1.01 g, 5.80 mmol) in CH_2Cl_2 (200 mL) at 23 °C. The solution was washed with a saturated aqueous $NaHCO_3$ solution, brine, dried over $MgSO_4$, and filtered. The solvent was evaporated, and the resulting solid was dissolved in toluene (200 mL). A suspension of DDQ (0.67 g, 2.9 mmol) in toluene (200 mL) was added, and the mixture was stirred for 1 h at 23 °C. Then, TEA (1.6 mL, 11 mmol) and BF_3·Et_2O (2.8 mL, 22 mmol) were added and the mixture was heated to 75 °C for 40 min. After cooling to 23 °C, the mixture was filtered through a plug of SiO_2, eluted with CH_2Cl_2 and the solvent was evaporated. The crude product was purified by FC (SiO_2; CH_2Cl_2/cyclohexane 1:1) to afford **29** (1.1 g, 1.9 mmol, 69%) as a dark green solid. R_f = 0.54 (SiO_2; CH_2Cl_2/cyclohexane 1:1); m.p.: 330–340 °C (decomp); ^{1}H NMR (400 MHz, $CDCl_3$): δ = 1.42 (s, 6H), 2.42 (s, 6H), 2.55 (t, J = 7.0 Hz, 4H), 2.89 (t, J = 7.0 Hz, 4H), 7.22 (s, 2H), 7.24–7.28 (m, 2H), 7.28–7.35 (m, 2H), 7.39–7.46 (m, 2H), 8.80 ppm (d, J = 8.0 Hz, 2H) ppm; ^{13}C NMR (101 MHz, $CDCl_3$): δ = 12.76, 17.69, 20.63, 30.63, 127.52, 128.27, 128.38, 128.88 (t, J = 11.6 Hz), 129.58, 129.77, 131.05, 132.52, 133.60, 135.63, 137.20, 138.42, 140.89, 151.35, 152.36 ppm; ^{19}F NMR (376 MHz, $CDCl_3$): δ = −135.06 ppm (q, J = 34.1 Hz); IR (ATR): $\tilde{\nu}$ = 2934, 2899, 2837, 2359, 2339, 1605, 1556, 1519, 1468, 1435, 1397, 1385, 1357, 1341, 1324, 1304, 1276, 1230, 1189, 1161, 1104, 1082, 1069, 1042, 1028, 1012, 950, 911, 893, 873, 866, 819, 779, 747, 732, 706, 676, 649, 633, 622 cm^{-1}; UV/Vis ($CHCl_3$): λ_{max} (ε) = 311 (15000), 316 (51000), 395 (10000), 573 (26000), 621 nm (116000); HR-MALDI-MS (3-HPA): m/z (%): 573.2406 (100) $[M]^+$ (calcd for $C_{35}H_{30}BF_2N_3O_2^+$: 573.2399), 554.2420 (47) $[M-F]^+$ (calcd for $C_{35}H_{30}BFN_3O_2^+$: 554.2415).

{4-[(4-Ethyl-3,5-dimethyl-1*H*-pyrrol-2-yl-κ*N*)(4-ethyl-3,5-dimethyl-2*H*-pyrrol-2-ylidene-κ*N*)methyl]-2,6-dimethylanilinato}(difluoro)boron (31): Hydrazine monohydrate (2.9 mL, 93 mmol) and Pd/C (10%, 0.49 g, 0.46 mmol) were added to a degassed solution of **28** (2.1 g, 4.6 mmol) in THF (50 mL) and EtOH (100 mL). The mixture was heated to reflux for 40 min, then cooled to 23 °C. Celite was added, and the mixture was filtered through a plug of Celite. The solvent was evaporated, and the residue was purified by FC (SiO_2; CH_2Cl_2/cyclohexane 1:1→4:1), affording **31** (1.8 g, 4.3 mmol, 92%) as a dark red solid. R_f = 0.20 (SiO_2; CH_2Cl_2/cyclohexane 3:1); m.p.: 240–245 °C; ^{1}H NMR (400 MHz, $CDCl_3$): δ = 0.99 (t, J = 7.6 Hz, 6H), 1.37 (s, 6H), 2.22 (s, 6H), 2.30 (q, J = 7.6 Hz, 4H), 2.52 (s, 6H), 3.72 ppm (s, 2H), 6.81 (s, 2H); ^{13}C NMR (101 MHz, $CDCl_3$): δ = 12.16, 12.58, 14.78, 17.23, 17.69, 122.34, 125.11, 128.06, 131.54, 132.44, 138.69, 141.75, 143.14, 153.05 ppm; ^{19}F NMR (376 MHz, $CDCl_3$): δ = −145.84 ppm (q, J = 33.3 Hz); IR (ATR): $\tilde{\nu}$ = 3493, 3410, 2969, 2926, 2869, 1623, 1539, 1474, 1403, 1388, 1371, 1313, 1258, 1184, 1159, 1113, 1076, 1038, 971, 867, 798, 756, 728, 705, 668, 637 cm^{-1}; UV/Vis ($CHCl_3$): λ_{max} (ε) = 379 (9000), 525 nm (79000); HR-MALDI-MS (3-HPA): m/z (%): 423.2643 (100) $[M]^+$ (calcd for $C_{25}H_{32}BF_2N_3^+$: 423.2657), 404.2656 (92) $[M-F]^+$ (calcd for $C_{25}H_{32}BFN_3^+$: 404.2673).

{2,6-Dimethyl-4-[(3-methyl-4,5-dihydro-1*H*-benzo[*g*]indol-2-yl-κ*N*)(3-methyl-4,5-dihydro-2*H*-benzo[*g*]indol-2-ylidene-κ*N*)methyl]anilinato}(difluoro)-boron (32): Hydrazine monohydrate (0.42 mL, 14 mmol) and Pd/C (10%, 0.29 g, 0.27 mmol) was added to a degassed solution of **29** (390 mg, 0.680 mmol) in THF (10 mL) and EtOH (20 mL),. The mixture was heated to reflux for 32 h. After cooling to 23 °C, Celite was added and the mixture was filtered through a plug of Celite. The solvent was evaporated, and the residue was purified by FC (SiO_2; CH_2Cl_2/cyclohexane

1:1), yielding **32** (190 mg, 0.349 mmol, 51%) as a dark red solid. $R_f = 0.38$ (SiO_2; CH_2Cl_2/cyclohexane 3:1); m.p.: 330–340°C (decomp.); ^{1}H NMR (400 MHz, $CDCl_3$): $\delta = 1.46$ (s, 6H), 2.25 (s, 6H), 2.54 (t, $J = 7.0$ Hz, 4H), 2.87 (t, $J = 7.0$ Hz, 4H), 3.77 (s, 2H), 6.90 (s, 2H), 7.21–7.31 (m, 4H), 7.38–7.44 (m, 2H), 8.80 ppm (d, $J = 8.0$ Hz, 2H) ppm; ^{13}C NMR (101 MHz, $CDCl_3$): $\delta = 12.63$, 17.69, 20.61, 30.73, 122.40, 125.43, 127.39, 128.10, 128.55, 128.70, 128.83, 129.20, 131.73, 134.79, 136.48, 140.62, 141.58, 143.47, 150.34 ppm; ^{19}F NMR (376 MHz, $CDCl_3$): $\delta = -134.79$ ppm (q, $J = 34.1$ Hz); IR (ATR): $\tilde{\nu} = 3486$, 3401, 3037, 2921, 2833, 1635, 1547, 1522, 1466, 1433, 1402, 1386, 1367, 1327, 1307, 1275, 1235, 1194, 1169, 1157, 1086, 1047, 1021, 976, 958, 944, 919, 876, 828, 750, 732, 720, 710, 683, 668, 632, 608 cm^{-1}; UV/Vis ($CHCl_3$): λ_{max} (ε) = 311 (53000), 401 (8000), 566 (24000), 613 nm (109000); HR-MALDI-MS (3-HPA): *m/z* (%): 543.2654 (100) $[M]^+$ (calcd for $C_{35}H_{32}BF_2N_3^+$: 543.2657), 524.2675 (39) $[M-F]^+$ (calcd for $C_{35}H_{32}BFN_3^+$: 524.2673).

Compound 34: K_2CO_3 (64 mg, 0.46 mmol) was added to a degassed solution of **12** (0.50 g, 0.46 mmol) and **13** (0.22 g, 0.35 mmol) in Me_2SO (30 mL). The mixture was stirred for 4 h at 23°C, after which it was poured into H_2O (300 mL). The resulting precipitate was collected by filtration, washed with H_2O (3×10 mL), and dried in vacuo. Recycling GPC (Jaigel-2H; $CHCl_3$) afforded **34** (43 mg, 0.026 mmol, 6%) as a red solid. $t_R = 21.8$ min (Jaigel-2H; $CHCl_3$, flow = 4 mL min^{-1}); m.p.: 250–260°C (decomp); ^{1}H NMR (400 MHz, $CDCl_3$): $\delta = 0.88$–0.96 (m, 12H), 1.05 (t, $J = 7.5$ Hz, 6H), 1.19 (s, 3H), 1.26 (s, 3H), 1.27–1.51 (m, 32H), 2.26 (s, 6H), 2.15–2.47 (m, 12H), 2.58 (s, 6H), 4.30 (t, $J = 7.7$ Hz, 1H), 5.62 (t, $J = 7.6$ Hz, 3H), 7.07 (s, 1H), 7.13 (s, 2H), 7.16 (s, 2H), 7.22 (s, 1H), 7.27–7.31 (m, 2H), 7.33 (s, 2H), 7.42 (t, $J = 7.7$ Hz, 2H), 7.68 (d, $J = 7.8$ Hz, 2H), 8.09 (d, $J = 8.3$ Hz, 2H), 8.31 ppm (s, 2H); ^{13}C NMR (101 MHz, $CDCl_3$): $\delta = 12.11$, 12.73, 14.22, 14.81, 17.31, 17.84, 18.34, 22.82, 28.06, 28.13, 29.49, 29.54, 29.85, 32.01, 32.02, 32.04, 32.51, 32.75, 33.75, 33.91, 34.17, 34.55, 110.83, 118.78, 123.76, 123.95, 127.34, 128.15, 128.67, 128.84, 129.17, 129.35, 129.57, 130.65, 130.75, 133.24, 135.72, 137.50, 137.60, 137.66, 138.29, 138.50, 138.95, 139.60, 139.96, 141.73, 151.45, 152.29, 152.63, 152.73, 152.80, 152.99, 154.33, 158.79, 161.28 ppm; ^{19}F NMR (376 MHz, $CDCl_3$): $\delta = -146.26$, -145.08 ppm; IR (ATR): $\tilde{\nu} = 3365$ (w, br), 2926, 2856, 2360, 2341, 1741, 1540, 1479, 1410, 1359, 1323, 1263, 1222, 1189, 1159, 1115, 1066, 1042, 978, 897, 862, 842, 796, 757, 728, 682, 668, 649, 604 cm^{-1}; UV/Vis ($CHCl_3$): λ_{max} (ε) = 528 nm (66000); HR-MALDI-MS (3-HPA): *m/z* (%): 1627.7922 (27) $[M]^+$ (calcd for $C_{99}H_{104}BF_2N_9O_{10}^+$: 1627.7967), 1608.7921 (100) $[M-F]^+$ (calcd for $C_{99}H_{104}BFN_9O_{10}^+$: 1608.7992).

Acknowledgements

This work was supported by a grant from the Swiss National Science Foundation (SNF). I.P. acknowledges the receipt of a Novartis Master Fellowship and a fellowship from the Studienstiftung des deutschen Volkes. B.B. is supported by a Kekulé fellowship of the Fonds der Chemischen Industrie. We thank Dr. Vladimir Azov (University of Bremen) for helpful discussions, and Dr. Melanie Chiu and Dr. Nicolas Marion for reviewing the manuscript.

[1] J. R. Moran, S. Karbach, D. J. Cram, *J. Am. Chem. Soc.* **1982**, *104*, 5826–5828.
[2] V. A. Azov, A. Beeby, M. Cacciarini, A. G. Cheetham, F. Diederich, M. Frei, J. K. Gimzewski, V. Gramlich, B. Hecht, B. Jaun, T. Latychevskaia, A. Lieb, Y. Lill, F. Marotti, A. Schlegel, R. R. Schlittler, P. J. Skinner, P. Seiler, Y. Yamakoshi, *Adv. Funct. Mater.* **2006**, *16*, 147–156.
[3] P. Roncucci, L. Pirondini, G. Paderni, C. Massera, E. Dalcanale, V. A. Azov, F. Diederich, *Chem. Eur. J.* **2006**, *12*, 4775–4784.
[4] V. A. Azov, B. Jaun, F. Diederich, *Helv. Chim. Acta* **2004**, *87*, 449–462.
[5] P. J. Skinner, A. G. Cheetham, A. Beeby, V. Gramlich, F. Diederich, *Helv. Chim. Acta* **2001**, *84*, 2146–2153.
[6] M. Frei, F. Marotti, F. Diederich, *Chem. Commun.* **2004**, 1362–1363.
[7] V. A. Azov, F. Diederich, Y. Lill, B. Hecht, *Helv. Chim. Acta* **2003**, *86*, 2149–2155.
[8] V. A. Azov, P. Skinner, Y. Yamakoshi, P. Seiler, V. Gramlich, F. Diederich, *Helv. Chim. Acta* **2003**, *86*, 3648–3670.
[9] V. A: Azov, A. Schlegel, F. Diederich, *Bull. Chem. Soc. Jpn.* **2006**, *79*, 1926–1940.
[10] P. P. Castro, G. Zhao, G. A. Masangkay, C. Hernandez, L. M. Gutierrez-Tunstad, *Org. Lett.* **2004**, *6*, 333–336.
[11] a) A. Burghart, H. Kim, M. B. Welch, L. H. Thoresen, J. Reibenspies, K. Burgess, F. Bergstrom, L. Johansson, *J. Org. Chem.* **1999**, *64*, 7813–7819; b) J. Chen, A. Burghart, A. Derecskei-Kovacs, K. Burgess, *J. Org. Chem.* **2000**, *65*, 2900–2906.
[12] For FRET studies of the dynamics of resorcin[4]arene derived self-assembled capsules, see: E. S. Barrett, T. J. Dale, J. Rebek, Jr., *J. Am. Chem. Soc.* **2007**, *129*, 3818–3819.
[13] V. A. Azov, A. Schlegel, F. Diederich, *Angew. Chem.* **2005**, *117*, 4711–4715; *Angew. Chem. Int. Ed.* **2005**, *44*, 4635–4638.
[14] L. D. Shirtcliff, H. Xu, F. Diederich, *Eur. J. Org. Chem.* **2010**, 846–855.
[15] Whereas crystals of **11** were yellow-green cubes, crystals of compound **16** were yellow-green plates. Both X-ray crystal structures show the cavitands as solvates with acetone inside the cavity of **11** and CH_2Cl_2 inside the cavity of **16** (Figure 1SI in the Supporting Information).
[16] O. Lavastre, L. Ollivier, P. H. Dixneuf, S. Sibandhit, *Tetrahedron* **1996**, *52*, 5495–5504.
[17] K. Hishikawa, H. Nakagawa, T. Furuta, K. Fukuhara, H. Tsumoto, T. Suzuki, N. Miyata, *J. Am. Chem. Soc.* **2009**, *131*, 7488–7489.
[18] A. Cui, X. Peng, J. Fan, X. Chen, Y. Wu, B. Guo, *J. Photochem. Photobiol. A* **2007**, *186*, 85–92.
[19] D. J. Cram, H. Choi, J. A. Bryant, C. B. Knobler, *J. Am. Chem. Soc.* **1992**, *114*, 7748–7765.
[20] J. Chen, J. Reibenspies, A. Derecskei-Kovacs, K. Burgess, *Chem. Commun.* **1999**, 2501–2502.
[21] For other examples, in which ^{19}F NMR spectroscopy has been used to study the conformations of BODIPY dyes, see: A. C. Benniston, G. Copley, A. Harriman, D. Howgego, R. W. Harrington, W. Clegg, *J. Org. Chem.* **2010**, *75*, 2018–2027, and references therein.
[22] Degradation of both dye moieties was observed at higher TFA concentrations (see Figure 11SI–13SI in the Supporting Information), whereby degradation of the acceptor was even faster than that of the donor. As a consequence of these findings, measurements of the fluorescence spectra in the titration experiments were performed as quickly as possible after mixing the cavitand with TFA (after ca. 20 s). Because slight degradation of the BODIPY-dye moieties could not be avoided, and because the acceptor dye degrades more quickly than the donor dye, the absolute FRET efficiencies for cavitands **1**–**4** are artificially low under these conditions. However, because a uniform experimental protocol was used throughout these measurements, the relative FRET efficiencies within the cavitand series are internally consistent.
[23] T. Förster, *Ann. Phys.* **1948**, *437*, 55–75.
[24] S. Watt, C. Dai, A. Scott, J. Burke, R. Thomas, J. Collings, C. Viney, W. Clegg, T. Marder, *Angew. Chem.* **2004**, *116*, 3123–3125; *Angew. Chem. Int. Ed.* **2004**, *43*, 3061–3063.
[25] P. Pagliusi, F. Lagugne-Labarthet, D. K. Shenoy, E. Dalcanale, Y. R. Shen, *J. Am. Chem. Soc.* **2006**, *128*, 12610–12611.
[26] A. Altomare, M. C. Burla, M. Camalli, G. L. Cascarano, C. Giacovazzo, A. Guagliardi, A. G. G. Moliterni, G. Polidori, R. Spagna, *J. Appl. Crystallogr.* **1999**, *32*, 115–119.
[27] G. M. Sheldrick, SHELXL-97, Program for the Refinement of Crystal Structures, University of Göttingen, Germany, **1997**.
[28] D. M. Doleib, Y. Iskander, *J. Chem. Soc. B* **1967**, 1154–1158.

Received: June 9, 2010
Published online: September 23, 2010

